

INFLUENCE OF FUNCTIONAL GROUPS ON THE PHOTODYNAMIC
THERAPY AND INTERNALIZATION OF PORPHYRIN MODIFIED POLYHEDRAL
OLIGOMERIC SILSESQUIOXANE (POSS) MOLECULES IN MAMMALIAN CELLS

by

Alexis Johnston

A thesis submitted to the faculty of
The University of North Carolina at Charlotte
In partial fulfillment of the requirements
for the degree of Master of Science in
Chemistry

Charlotte

2020

Approved by:

Dr. Juan L. Vivero-Escoto

Dr. Nathaniel Fried

Dr. Tom Schmedake

Dr. Jerry Troutman

©2020
Alexis Johnston
ALL RIGHTS RESERVED

ABSTRACT

ALEXIS JOHNSTON. Influence of functional groups on the photodynamic therapy and internalization of porphyrin-modified polyhedral oligomeric silsesquioxane molecules in mammalian cells. (Under the direction of Dr. JUAN L. VIVERO-ESCOTO)

Polyhedral Oligomeric Silsesquioxane (POSS) molecules are highly ordered organic-inorganic hybrid materials with a cage like core of alternating silicon and oxygen atoms surrounded by eight pedant organic residues. These compounds are well-defined, 3D building blocks that can form hybrid materials with precise control of the nanostructure and properties. POSS molecules are used in a wide variety of medical fields, for example, tissue engineering and drug delivery, or for the oligomerization of bioactive ligands, among them peptides and carbohydrates. They are considered non-toxic and hydrolytic degradation of the inorganic core under physiological conditions has been thoroughly investigated. In this work, we have taken advantage of the chemical and structural properties of POSS to functionalize this material with porphyrin. Moreover, the corner groups have been functionalized with either isobutyl or phenyl groups. We hypothesize that the differences in surface functionalization will have a major impact on the internalization and phototoxicity and of POSS-Porphyrin against mammalian cancer cells. Further studies will expand the scope of this investigation with drug-conjugated POSS molecules and target-specific systems.

DEDICATION

This thesis is dedicated to my family, loved ones, and friends. Without their unyielding support, encouragement, and love none of this would be possible. Thank you for providing me with the strength and guidance I needed to persevere.

ACKNOWLEDGEMENTS

I would like to express my deepest appreciation to my advisor, Dr. Juan L. Vivero-Escoto. I am extremely grateful for his dedicated guidance, support, patience and encouragement throughout my time in the lab. His influential mentorship helped me with my research project and with the structure and the writing of this thesis. I would also like to thank my thesis committee: Dr. Nathaniel Fried, Dr. Tom Schmedake, and Dr. Jerry Troutman, for their time and intellectual contributions. A special thanks to Dr. Markus Etzkorn for his guidance throughout the program and to the UNCC Biology department, specifically Dr. Didier Dréau for his instrumental assistance with my project. Lastly, I would like to thank the members of the V-Lab and my colleagues for their help and support over the past few years.

TABLE OF CONTENTS

LIST OF TABLES	ix
LIST OF FIGURES	x
LIST OF ABBREVIATIONS.....	xi
CHAPTER 1: INTRODUCTION.....	1
1.1 Use of Nanoparticles for Drug Delivery	1
1.2 Nanoclusters as a Promising Option for Drug Delivery	2
1.3 Polyhedral Oligomeric Silsesquioxane (POSS) Nanoclusters.....	3
1.4 Biomedical Applications of POSS Nanoclusters.....	4
1.4.1 Drug delivery	4
1.5 Hypothesis and Aims	5
CHAPTER 2: POSS-PORPHYRIN FOR PHOTODYNAMIC THERAPY	7
2.1 Introduction.....	7
2.1.1 Basic Principles of Photodynamic Therapy (PDT).....	7
2.1.2 Photosensitizers.....	8
2.1.3 Applications of POSS for PDT	9
2.1.4 Hypothesis and Aims	10
2.2 Experiments	10
2.2.1 Synthesis and characterization of aminopropyl hepta(isobutyl) POSS (1-(3-amino)propyl-3,5,7,9,11,13,15-heptaisobutylpentacyclo[9.5.1.1(3,9).1(5,15).1(7,13)]octasiloxane) (AP-IB-POSS).....	10
2.2.2 Synthesis and characterization of isocyanato propyl hepta(isobutyl) POSS (1-isocyanatopropyl-3,5,7,9,11,13,15-heptaisobutyl pentacyclo[9.5.1.1(3,9).1(5,15).1(7,13)]octasiloxane) (IP-IB-POSS)	11

2.2.3 Synthesis and characterization of hepta(isobutyl)-POSS-Porphyrin (5-(4-[3-(3-(3,5,7,9,11,13,15-heptaisobutyl pentacyclo[9.5.1.1(3,9).1(5,15).1(7,13)] octasiloxane) propyl) ureido] phenyl)-10,15,20-(triphenyl)porphyrin) (IB-POSS-Porphyrin).....	12
2.2.4 Synthesis and characterization of aminopropyl hepta(phenyl) POSS (1-(3-amino)propyl-3,5,7,9,11,13,15-heptaphenylpentacyclo[9.5.1.1(3,9).1(5,15).1(7,13)]octasiloxane) (AP-Ph-POSS)	13
2.2.5 Synthesis and characterization of isocyanato propyl hepta(phenyl) POSS (1-isocyanatopropyl-3,5,7,9,11,13,15-heptaphenyl pentacyclo[9.5.1.1(3,9).1(5,15).1(7,13)]octasiloxane (IP-Ph-POSS)	13
2.2.6 Synthesis and characterization of hepta(phenyl)-POSS-Porphyrin (5-(4-[3-(3-(3,5,7,9,11,13,15-heptaphenylpentacyclo[9.5.1.1(3,9).1(5,15).1(7,13)] octasiloxane)propyl) ureido] phenyl)-10,15,20-(triphenyl)porphyrin) (Ph-POSS-Porphyrin).....	14
2.2.7 Synthesis and characterization of (tetra-(4-[3-(3-(3,5,7,9,11,13,15-heptaisobutyl pentacyclo[9.5.1.1(3,9).1(5,15).1(7,13)]octasiloxane) propyl) ureido] phenyl)-10,15,20-(triphenyl)porphyrin) (tet(IB-POSS)-Porphyrin)	15
2.2.8 Photophysical characterization	15
2.2.8.1 UV-VIS/Fluorescence Spectroscopy	15
2.2.8.2 Fluorescence Quantum Yield.....	16
2.2.8.3 Singlet Oxygen Quantum Yield.....	17
2.2.9 Cell Culture	17
2.2.10 <i>In vitro</i> PDT Evaluation.....	18
2.2.11 Flow Cytometry	19
2.3 Results and Discussion	20
2.3.1 Synthesis and characterization of POSS-Porphyrin.....	20
2.3.2 Photophysical Characterization	22
2.3.3 PDT using POSS-Porphyrin	25
2.3.4 Flow cytometry	27

2.4 Conclusions and Future Work	28
CHAPTER 3: INTERNALIZATION OF POSS IN MAMMALIAN CELLS	30
3.1 Introduction	30
3.1.1 Mechanism for Cellular Internalization of Molecules	30
3.1.2 Mechanism for Cellular Internalization of Nanoparticles	30
3.1.3 Mechanism for Cellular Internalization of POSS	31
3.1.4 Hypothesis and Aims	31
3.2 Experiments	32
3.2.1 Synthesis and Characterization of isobutyl-POSS-fluorescein (IB-POSS-fluorescein)	32
3.2.2 Synthesis and Characterization of phenyl-POSS-fluorescein (Ph-POSS-fluorescein)	33
3.2.3 Photophysical Characterization	33
3.2.4 Toxicity of POSS-fluorescein	34
3.2.5 Temperature-dependent Internalization of POSS	35
3.3 Results and Discussion	36
3.3.1 Synthesis and Characterization of POSS-fluorescein	36
3.3.2 Photophysical Characterization Toxicity of POSS-fluorescein	37
3.3.3 Toxicity of POSS-fluorescein	37
3.3.4 Mechanism of Cellular Internalization of POSS-fluorescein	38
3.4 Conclusions and Future Work	39
CHAPTER 4: CONCLUSIONS AND FUTURE WORK	41
REFERENCES	43
APPENDIX	49

LIST OF TABLES

TABLE 1. Photophysical and photochemical properties of POSS-Porphyrins

TABLE 2. Porphyrin and POSS-Porphyrin cell viability percentage at 0.5 μM

LIST OF FIGURES

FIGURE 1. Molecular structure of POSS. The letter 'R' denotes an organic substituent.

FIGURE 2. Molecular structure of POSS-Porphyrin nanoclusters. The porphyrin will be functionalized with isobutyl, phenyl, and tetra(isobutyl POSS).

FIGURE 3. Molecular structure of POSS-fluorescein nanoclusters. Fluorescein will be functionalized with isobutyl and phenyl POSS.

FIGURE 4. Photodynamic Therapy Diagram. Following irradiation of a photosensitizer with a specific wavelength of light, the photosensitizer is promoted to the excited singlet state (PS_{ES}). From here, the photosensitizer is converted to the excited triplet state (PS_{ET}) through intersystem crossing. Reaction of the photosensitizer with oxygen and biomolecules results in the production of reactive oxygen species (ROS).²⁸

FIGURE 5. Molecular structure of Isobutyl-POSS-Porphyrin, Phenyl-POSS-Porphyrin, and tetra(Isobutyl-POSS)-Porphyrin.

FIGURE 6. (A) Normalized absorption and (B) emission spectra for 6.6 μM solutions of Porphyrin (red), IB-POSS-Porphyrin (green), Ph-POSS-Porphyrin (purple), and tet(IB-POSS)-Porphyrin (black) in THF. The four Q absorption bands are shown in the inset.

FIGURE 7. Phototoxicity of Porphyrin (red), IB-POSS-Porphyrin (green), Ph-POSS-Porphyrin (purple), and tet(IB-POSS)-Porphyrin (orange).

FIGURE 8. Cytotoxicity of Porphyrin (red), IB-POSS-Porphyrin (green), Ph-POSS-Porphyrin (purple), and tet(IB-POSS)-Porphyrin (orange).

FIGURE 9. Internalization of POSS-Porphyrin molecules at 0.1 and 0.5 μM (IB is for IB-POSS-Porphyrin and Ph is for Ph-POSS-Porphyrin).

FIGURE 10. Molecular structure of IB-POSS-fluorescein and Ph-POSS-fluorescein.

FIGURE 11. UV-VIS spectrum of IB-POSS-fluorescein and Ph-POSS-fluorescein (green is for IB-POSS-fluorescein and purple is for Ph-POSS-fluorescein).

FIGURE 12. Cytotoxicity of POSS-fluorescein compounds (green is for IB-POSS-fluorescein, purple is for Ph-POSS-fluorescein, and orange is for fluorescein).

FIGURE 13. Temperature-dependent internalization of IB-POSS-fluorescein and Ph-POSS-fluorescein (5 and 10 μM in DMSO) (blue is for 4° C and red is for 37° C).

LIST OF ABBREVIATIONS

AP-IB-POSS	Aminopropyl hepta(isobutyl) POSS
AP-Ph-POSS	Aminopropyl hepta(phenyl) POSS
APTES	(3-aminopropyl) triethoxysilane
DCM	Dichloromethane
DIPEA	Diisopropylethylamine
DMSO	Dimethyl Sulfoxide
EC ₅₀	Half Maximal Effective Concentration
IB-POSS-fluorescein	Hepta(isobutyl)-POSS-fluorescein
IB-POSS-Porphyrin	Hepta(isobutyl)-POSS-Porphyrin
IP-IB-POSS	Isocyanato propyl hepta(isobutyl)-POSS
IP-Ph-POSS	Isocyanato propyl hepta(phenyl)-POSS
ISC	Intersystem Crossing
NP	Nanoparticle
PBS	Phosphate Buffer Saline
PDT	Photodynamic Therapy
Ph-POSS-fluorescein	Hepta(phenyl)-POSS-fluorescein
Ph-POSS-Porphyrin	Hepta(phenyl)-POSS-Porphyrin
Porphyrin	5-(4-aminophenyl)-10,15,20-(triphenyl)porphyrin
POSS	Polyhedral Oligomeric Silsesquioxane
PS	Photosensitizer
RFI	Relative Fluorescence Intensity
TAPP	5,10,15,20-tetra(4-aminophenyl)porphyrin

Tet(IB-POSS)-Porphyrin

Tetra(hepta(isobutyl)-POSS)-Porphyrin

THF

Tetrahydrofuran

TMAOH

Tetramethylammonium hydroxide

TPP

Tetraphenylporphyrin

CHAPTER 1: INTRODUCTION

1.1 Use of Nanoparticles for Drug Delivery

Conventional techniques for the administration of drugs are usually associated with low therapeutic indices and short half-lives.¹ The active ingredients in drugs administered through this method often react with non-targeted receptors inducing highly toxic side effects.¹ In the past few decades, targeted and controlled-release drug delivery systems have aided in enhancing the efficacy of commercially-available drugs and given rise to the production of new drug and therapy development.²

Nanoparticulate drug delivery systems have emerged as a more efficient way to deliver drugs than traditional methods. By definition, nanoparticles range from 1-100 nm in size. Optimization of their size and shape allows for the controlled release of drugs and their possible surface modifications further allows for increased solubility and absorption across biological barriers.³

The properties and performance of nanoparticles include, polymers, liposomes, lipids, capsules, dendrimers, and protein-based particles depending on the desired outcome.⁴ These nanoparticles can be used to increase drug stability, targeting, or circulation due to small size. In addition, inorganic nanoparticles are increasingly becoming known for their hydrophilicity, tunability, and stability compared to organic nanoparticles.⁵ Iron oxide, calcium phosphate, silica, gold, and silver nanoparticles are among the most commonly used as drug carriers.⁵

Some of the disadvantages associated with using nanoparticles as drug delivery systems include the inability to fine tune and control the amount of surface ligands added to the nanoparticle leading to difficulty with precise characterization. In addition,

nanoparticles internalized through endocytic pathways can become trapped within the endolysosomal pathway leading to degradation before drug release. Their size also facilitates accumulation in the liver reducing the overall efficacy of the drug and increasing the hepatic toxicity.⁶ Therefore, new alternatives for drug delivery systems are needed.

1.2 Nanoclusters as a Promising Option for Drug Delivery

To overcome the limitations above mentioned associated with using nanoparticles for drug delivery, some researchers have explored the use of nanoclusters. Nanoclusters consist of a small number of atoms, are composed either of a single or multiple element, and typically measure less than 2 nm.⁷ Their small hydrodynamic diameters allow for high accumulation in tumors and is ideal to reduce side effects upon renal excretion.⁸

In particular, metal nanoclusters specifically have high luminescence efficiency, toxicity, and photo-stability making them good candidates for labeling and drug delivery.^{8,9} Silver and gold nanoclusters are among the most commonly used platforms for drug delivery and diagnosis.⁹ Both of these metal nanoclusters show exceptional physical and chemical properties including tunable fluorescence, high quantum yields and biocompatibility.⁹ These nanoclusters can be conjugated to anticancer drugs through their surface ligands making them an ideal theranostic for cancer therapies.⁷ Gold nanoclusters have been successfully loaded with drugs for selective tumor diagnosis and treatment *in vivo*.¹⁰ Silver nanoclusters are less widely used due to their susceptibility to oxidation. Despite this, they have been effectively used for cancer cell and tumor imaging as well as a sensitizer in photodynamic therapy.¹¹ Metal nanoclusters, although more

biocompatible than nanoparticles, still possess similar limitations such as difficulties with characterization and functionalization.

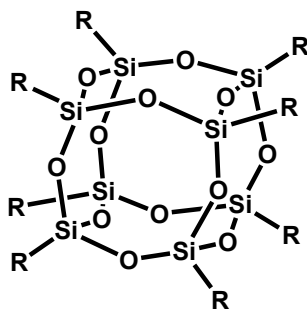


Figure 1. Molecular structure of POSS. The letter ‘R’ denotes an organic substituent.

1.3 Polyhedral Oligomeric Silsesquioxane (POSS) Nanoclusters

POSS nanoclusters are another interesting alternative for their use in drug delivery and diagnosis. POSS range from 1-3 nm in diameter and are composed of an inorganic siloxane core arranged in a 3-dimensional cage conformation (**Figure 1**).¹² These molecules can have 8-16 silicon atoms in the core; but, cages with 8 silicon atoms are most stable.¹³ Considering the well-known silicon chemistry, POSS can be easily functionalized at the eight corners. In addition, functional groups added to the POSS can also be modified, making this nanocluster a tunable toolkit as a building block to develop novel delivery systems.¹⁴ POSS nanoclusters can be hydrolytically stable depending on the substituents added and the surrounding chemical environment and are known to have low toxicity.¹⁴ In this thesis, we took advantage of the tunability of POSS nanoclusters to evaluate their performance in photodynamic therapy.

1.4 Biomedical Applications of POSS nanoclusters

POSS have been used in tissue engineering, molecular probing, and diagnostic techniques. Polymerizing POSS with carbohydrates and peptides have been investigated for tissue engineering.^{2, 15} In cartilage tissue engineering, POSS has been incorporated into the synthetic polymer polycarbonate urethane (POSS-PCU) to enhance both the thermal stability and biocompatibility of the polymer.¹⁶ POSS-PCU has demonstrated successful treatment of advanced tracheal cancer.¹⁶ Moreover, fluorinated ligands have been added to the POSS core for use as molecular probes to calculate enzymatic activity in tumor cells.¹⁷ This was advantageous because it eliminated the need for heavy metals.¹⁷ Oligoelectrolyte POSS derivatives incorporated into polymeric nanoparticles have been used for targeted tumor imaging and nuclear-staining agents for enhanced DNA labeling.¹⁸

1.4.1 Drug Delivery

The use of POSS as a drug delivery system *in vitro* has recently been studied. Their low toxicity, biocompatibility and nanoscale size have made them ideal candidates as drug carriers.¹⁹ Four general approaches have been identified: 1) Cell membrane penetration, which is achieved when the substituents are positively charged allowing the cationic molecule to diffuse through a membrane.²⁰ 2) The synthesis of amphiphilic POSS nanoclusters enabling the self-assembly of micelle-like structures that can be internalized by cells.²¹ 3) Addition of branched substituents to make the molecule a dendrimer.²² Peptide dendrimers are most often used because of their biodegradability and immobilization of drugs on peripheral functional groups. 4) POSS nanoclusters have the ability to be incorporated into biocompatible polymers such as polyethylene glycol.²³

Interestingly, in the first approach, only functional groups with positive charge have been investigated; however, no other functional groups have been explored.

1.5 Hypothesis and Aims

We hypothesize that tuning the chemical properties of POSS nanoclusters with different functional groups will impact their performance for biomedical applications. In this thesis, we were interested in studying the effect of hydrophobic groups on the photodynamic therapy and internalization of POSS nanoclusters in cancer cells. The following Aims were pursued in this thesis:

Aim 1: Three POSS nanoclusters containing a photosensitizer with different functional groups were synthesized, and the structural and photophysical properties characterized (**Figure 2**). The internalization and phototoxicity of these POSS-porphyrin nanoclusters were tested on a triple negative breast cancer cell line.

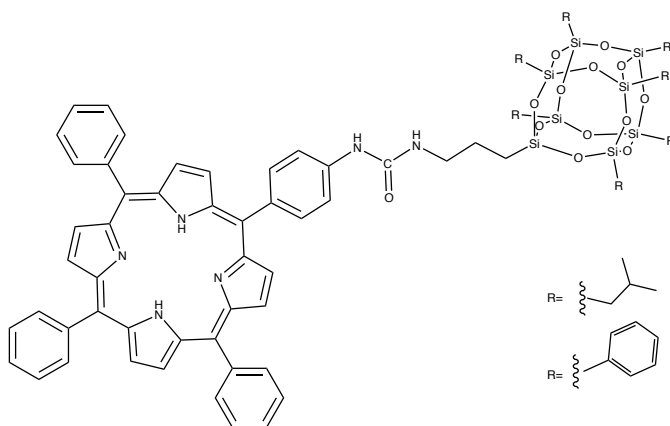


Figure 2. Molecular structure of POSS-Porphyrin nanoclusters. The porphyrin will be functionalized with isobutyl, phenyl, and tetra(isobutyl) POSS.

Aim 2: Two POSS nanoclusters containing a fluorophore with different functional groups were synthesized, and the structural and photophysical properties characterized (**Figure 3**). The method of internalization was partially investigated using flow cytometry.

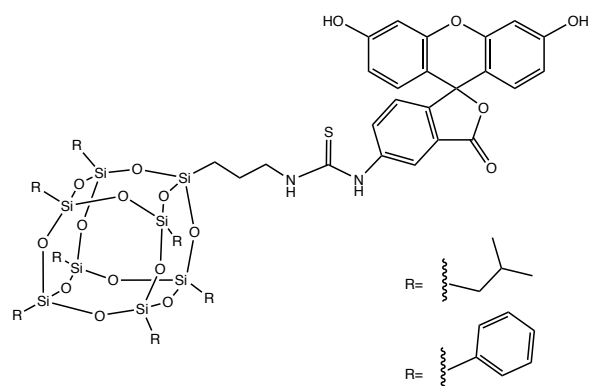


Figure 3. Molecular structure of POSS-fluorescein nanoclusters. Fluorescein will be functionalized with isobutyl and phenyl POSS.

CHAPTER 2: POSS-PORPHYRIN FOR PHOTODYNAMIC THERAPY

The work in this chapter would not be complete without the contributions of Paula Loman-Cortes and Paolo Siano. Paula Loman-Cortes completed the synthesis of isocyanato propyl hepta(isobutyl) POSS, hepta(isobutyl)-POSS-Porphyrin, isocyanato propyl hepta(phenyl) POSS, and hepta(phenyl)-POSS-Porphyrin. Paolo Siano completed the photophysical characterization of the POSS-Porphyrin molecules.

2.1 Introduction

2.1.1 Basic Principles of Photodynamic Therapy

A specific therapeutic approach focused on in this research is photodynamic therapy (PDT). PDT is a technique known for its clinical application as a treatment for malignant cells. This method involves the irradiation of a photosensitizing agent at the wavelength of absorption (**Figure 4**).²⁴ Photosensitizers (PSs) are light absorbing molecules that are nontoxic in the absence of light. Ideally, their absorption wavelength will be greater than 600 nm corresponding to deeper optical penetration through biological membranes.²⁵ The three key components necessary for PDT are a light source, PS and oxygen.²⁶ Upon irradiation with light, the PS is excited to its singlet state from which it undergoes intersystem crossing to the long-lived triplet state allowing for two possible photochemical reactions to occur, type I and type II.²⁷ Type I reactions involve the conversion of biomolecules, such as lipids and proteins, to hydroxyl radicals, superoxide radicals, and peroxide.²⁷ Type II reactions involve the conversion of oxygen to singlet oxygen.²⁷ The products produced from both type I and II reactions result in cell

death. The production of singlet oxygen from type II reactions is the driving force in PDT.

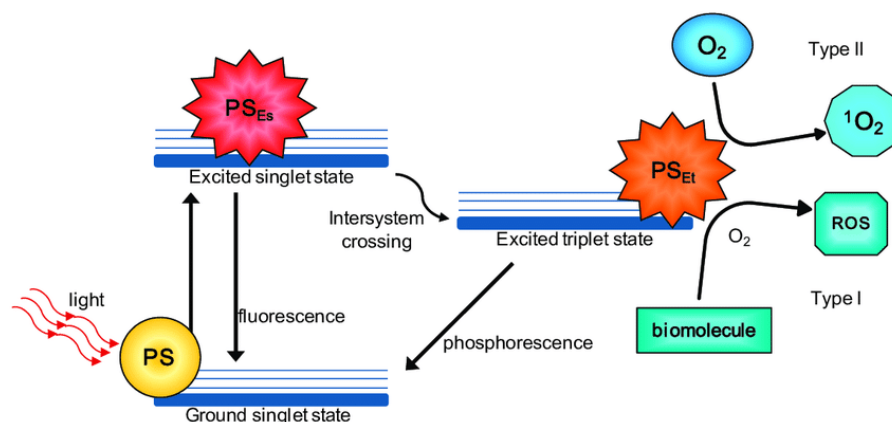


Figure 4. Photodynamic Therapy Diagram. Following irradiation of a photosensitizer with a specific wavelength of light, the photosensitizer is promoted to the excited singlet state (PS_{ES}). From here, the photosensitizer is converted to the excited triplet state (PS_{ET}) through intersystem crossing. Reaction of the photosensitizer with oxygen and biomolecules results in the production of reactive oxygen species (ROS).²⁸

2.1.2 Photosensitizers

Chlorins, phthalocyanines, and porphyrins are among many common tetrapyrrole photosensitizers studied for PDT.²⁹ Irradiation of these molecules have proven phototoxicity against solid tumors including triple negative breast cancer, lung, and pancreatic cancer cells.³⁰ Photofrin, Foscan, and Photochlor are approved photosensitizers used for the PDT treatment of various cancers.³¹ The use of these molecules is better due to the minimally invasive procedure needed, and the utilization of red light for irradiation.³² Although these molecules have been determined to be useful for PDT, their poor solubility leads to aggregation in aqueous media. Aggregation leads to self-quenching reducing generation of reactive oxygen species and the overall efficacy of PDT.³³

2.1.3 Applications of POSS for PDT

POSS compounds combined with porphyrins or chlorins have recently been used as scaffolds to develop nanoparticles for photodynamic therapy (PDT). Wu et. al modified POSS with chlorin e6 (Ce6) and polyethylene glycol (PEG) to produce POSS-Ce6-PEG with a high content of Ce6 (19.8 wt%) and remarkable anticancer efficiency with 95% cell death after 7 min under light irradiation against HeLa cells and a U14 xenograft mice model.³⁴ Kim et. al. also fabricated nanoparticles using POSS-Ce6 modified with a cancer-targeting peptide. This POSS-Ce6 platform was successfully evaluated *in vitro* and *in vivo* against triple-negative breast cancer (MDA-MB-231 cells).³⁵ In another approach, Zhang et. al. prepared a block copolymer using POSS and 4-vinylbenzyl-terminated tetraphenylporphyrin as the monomers. The self-assembly of this copolymer afforded nanoparticles with high photochemical yield and phototoxicity in a lung cancer model.³⁶ In a recent report, Wang et. al. demonstrated the use of a tetra-PEG-POSS substituted porphyrin for PDT treatment of cervical cancer *in vitro* and *in vivo*. The platform showed higher water solubility, good PDT efficiency, and better anticancer performance compared to Foscan.³⁷ Despite these inspiring works; to the best of our knowledge, the literature lacks a systematic investigation that focuses on the effects of different functional groups on the silsesquioxane cage of POSS-Porphyrin system for PDT.

2.1.4 Hypothesis and Aims

We hypothesize that tuning the chemical properties of POSS nanoclusters with different functional groups will impact their performance for photodynamic therapy. In this project, we investigated the performance of three polyhedral oligomeric silsesquioxane porphyrin (POSS-Porphyrin) compounds toward PDT (**Figure 5**). These POSS-Porphyrin molecules were rationally designed to contain different functional groups such as alkyl (isobutyl) and aromatic (phenyl); moreover, to evaluate the steric effect, a tetra-POSS substituted compound was also designed.

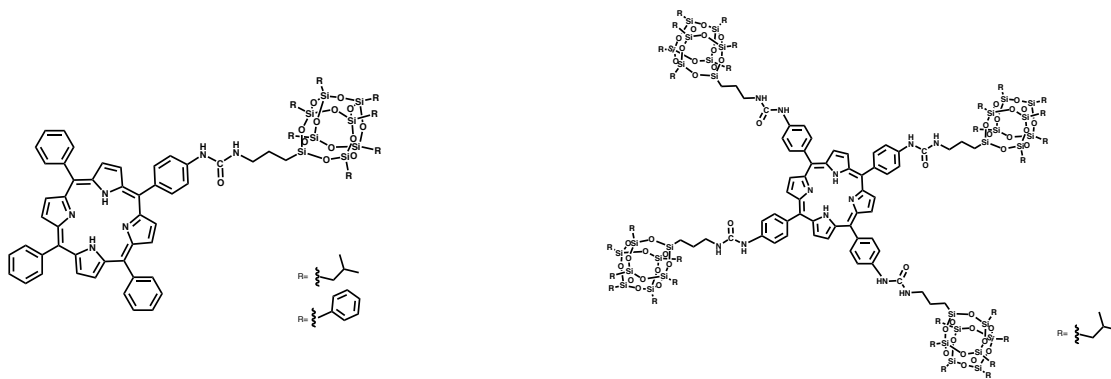


Figure 5. Molecular structure of Isobutyl-POSS-Porphyrin, Phenyl-POSS-Porphyrin, and tetra(Isobutyl-POSS)-Porphyrin.

2.2 Experiments

2.2.1 Synthesis of Aminopropyl hepta(isobutyl) POSS (1-(3-amino)propyl-

3,5,7,9,11,13,15-hepta(isobutyl) pentacyclo[9.5.1.1(3,9).1(5,15).1(7,13)]octasiloxane) (AP-IB-POSS)

The synthesis of AP-IB-POSS was carried out as previously reported with slight modifications.³⁸ Trisilanol hepta(isobutyl) POSS (2.00 g, 2.52 mmol) was dispersed in ethanol (12.5 mL) under stirring (550 rpm) followed by the addition of APTES (424 μ L, 435 mg, 1.97 mmol) and TMAOH (40 μ L, 0.06 mmol, 25% w/v). The mixture was

stirred (700 rpm) for 43 h at 40°C. A significant amount of aminopropyl hepta(isobutyl) POSS precipitated during the reaction time. The dispersion was centrifuged and the supernatant discarded. The solid product was washed twice with acetonitrile. The product was dried under vacuum for 48 h (Yield = 84% wt).

$^1\text{H-NMR}$ (300 MHz, CDCl_3 , ppm) δ : 2.78 (t, 2H, $-\text{CH}_2\text{-N-}$), 1.85 (m, 7H, $-\text{CH-}$), 1.66 (m, 2H, $-\text{CH}_2\text{-}$), 0.94 (d, 42H, CH_3), 0.60 (m, 16H, $-\text{Si-CH}_2\text{-}$); $^{29}\text{Si-NMR}$ (500 MHz, CDCl_3 , ppm) δ : -66.8, -67.2, -67.4. FTIR (cm^{-1}): 2953, 2906 and 2870 (C-H), 1600 (N-H), 1465 (C-N), 1228 (Si-C), 1081 (Si-O-Si), 955 (Si-O-Si), 740 (Si-C). MALDI-TOF (m/z): $[\text{M}]^+$ = 874.0 observed; $[\text{M}]^+$ = 873.31 calculated.

2.2.2 Synthesis of isocyanato propyl hepta(isobutyl) POSS (1-isocyanatopropyl-3,5,7,9,11,13,15-heptaisobutyl pentacyclo[9.5.1.1(3,9).1(5,15).1(7,13)]octasiloxane) (IP-IB-POSS)

The synthesis of IP-IB-POSS was carried out as previously reported with slight modifications.³⁹ Compound AP-IB-POSS (150 mg, 0.172 mmol) was dissolved in dry dichloromethane (2 mL) at room temperature and the solution was stirred slowly (300 rpm) under nitrogen atmosphere. DIPEA (60 μL , 44.5 mg, 0.34 mmol) and triphosgene (25.5 mg, 0.086 mmol) were added to this solution under slow stirring and N_2 atmosphere. After 3 h, the stirring speed and the nitrogen flow were increased to cause the evaporation of the solvent (evaporation time: 10 min). The product was washed twice with acetonitrile. Compound IP-IB-POSS was dried under vacuum for 48 h (Yield = 71% wt).

$^1\text{H-NMR}$ (300 MHz, CDCl_3 , ppm) δ : 3.28 (t, 2H, $-\text{CH}_2-\text{N}=\text{C}=\text{O}$), 1.85 (m, 7H, $-\text{CH}-$), 1.71 (m, 2H, $-\text{CH}_2-$), 0.94 (d, 42H, CH_3), 0.66 (t, 2H, $-\text{Si}-\text{CH}_2-$), 0.60 (m, 14H, $-\text{Si}-\text{CH}_2-$); $^{29}\text{Si-NMR}$ (500 MHz, CDCl_3 ppm) δ : -67.1, -67.4, -67.7. FTIR (cm^{-1}): 2954 and 2870 (C-H), 2273 (N=C=O), 1465 (C-N), 1229 (Si-C), 1084 (Si-O-Si), 955 (Si-O-Si), 739 (Si-C).

2.2.3 Synthesis of hepta(isobutyl)-POSS-Porphyrin (5-(4-[3-(3-(3,5,7,9,11,13,15-heptaisobutyl pentacyclo[9.5.1.1(3,9).1(5,15).1(7,13)]octasiloxane) propyl) ureido] phenyl)-10,15,20-(triphenyl)porphyrin) (IB-POSS-Porphyrin)

IB-POSS-Porphyrin (20 mg, 0.022 mmol) was dissolved in dry dichloromethane (2 mL) at room temperature. To this solution, 5-(4-aminophenyl)-10,15,20-(triphenyl)porphyrin (Porphyrin) (28 mg, 0.045 mmol) and excess DIPEA were added. The final solution was stirred at room temperature for 48 h in a sealed flask. The product was separated using column chromatography on silica gel (DCM:MeOH; 99:1). After purification, IB-POSS-Porphyrin was dried and obtained as a dark powder (Yield = 82 % wt).

$^1\text{H-NMR}$ (300 MHz, CDCl_3 , ppm) δ : 8.87 (m, 8H, Py-H), 8.18 (m, 8H, Ph-H), 7.74 (m, 11H, Ph-H), 3.34 (t, 2H, $-\text{CH}_2-\text{N}-$), 1.88 (m, 7H, $-\text{CH}-$), 1.76 (m, 2H, $-\text{CH}_2-$), 0.96 (d, 42H, CH_3), 0.71 (t, 2H, $-\text{Si}-\text{CH}_2-$), 0.61 (m, 14H, $-\text{Si}-\text{CH}_2-$); $^{29}\text{Si-NMR}$ (500 MHz, CDCl_3 , ppm) δ : -67.0, -67.1, -67.3. FTIR (cm^{-1}): 3318 (N-H), 2925 and 2870 (C-H), 1655 (C=O), 1465 (C-N), 1227 (Si-C), 1084 (Si-O-Si), 966 (Si-O-Si), 700 (Si-C). MALDI-TOF (m/z): $[\text{M}-1]^+ = 1527.55$ observed; $[\text{M}]^+ = 1528.55$ calculated.

2.2.4 Synthesis of Aminopropyl hepta(phenyl) POSS (1-(3-amino)propyl-3,5,7,9,11,13,15-heptaphenyl pentacyclo[9.5.1.1(3,9).1(5,15).1(7,13)]octasiloxane (AP-Ph-POSS)

The synthesis of AP-Ph-POSS was carried out as previously reported with slight modifications.⁴⁰ Trisilanol hepta(phenyl) POSS (2.48 gr, 2.7 mmol) was dispersed under stirring (500 rpm) in toluene (4.0 mL) and placed in a dry ice/acetone bath at -10 °C for 5 min. To this solution APTES (616 μ L, 600 mg, 2.7 mmol) was added. The final dispersion was let warm up to room temperature under stirring (500 rpm) for 16.5 h. Later, acetonitrile (20 mL) was added to precipitate the product. Finally, the supernatant was removed after centrifugation and the final product was washed twice with acetonitrile. AP-Ph-POSS was dried under vacuum for 48 h (Yield = 61% wt).

¹H-NMR (300 MHz, CDCl₃, ppm) δ : 7.74 (m, 14H, Ph-H), 7.44 (m, 7H, Ph-H), 7.37 (m, 14H, Ph-H), 2.66 (t, 2H, -CH₂-N-), 1.62 (m, 2H, -CH₂-), 0.84 (t, 2H, -Si-CH₂-); ²⁹Si-NMR (500 MHz, CDCl₃, ppm) δ : -64.5, -77.8, -78.3. FTIR (cm⁻¹): 3073 (N-H), 3051 (C-H, sp²), 2921 (C-H, sp³), 1595 (N-H), 1431 (C-N), 1082 (Si-O-Si), 1027 (Si-O-Si), 780 (Si-C). MALDI-TOF (m/z): [M]⁺ = 1014.60 observed; [M]⁺ = 1013.29 calculated.

2.2.5 Synthesis of isocyanato propyl hepta(phenyl) POSS (1-isocyanatopropyl-3,5,7,9,11,13,15-heptaphenyl pentacyclo[9.5.1.1(3,9).1(5,15).1(7,13)]octasiloxane (IP-Ph-POSS)

AP-Ph-POSS (174 mg, 0.172 mmol) was dissolved in dry dichloromethane (2 mL) at room temperature and the solution was stirred slowly (300 rpm) under nitrogen atmosphere. Triphosgene (25.5 mg, 0.086 mmol) and DIPEA (60 μ L, 44.5 mg, .34

mmol) were added to this solution under slow stirring and N₂ atmosphere. After 3 h, the stirring speed and the nitrogen flow were increased to cause the evaporation of the solvent (evaporation time: 10 min). The product was washed twice with acetonitrile twice. IP-Ph-POSS was dried under vacuum for 48 h (Yield = 78% wt).

¹H-NMR (300 MHz, CDCl₃, ppm) δ: 7.71 (m, 14H, Ph-H), 7.41 (m, 7H, Ph-H), 7.38 (m, 14H, Ph-H), 3.18 (m, 2H, -CH₂-N=C=O), 1.80 (m, 2H, -CH₂-), 0.84 (m, 2H, -Si-CH₂-); ²⁹Si-NMR (500 MHz, CDCl₃, ppm) δ: -65.3, -77.6, -78.1. FTIR (cm⁻¹): 3073 (C-H, sp²), 2933 (C-H, sp³), 2271 (N=C=O), 1600 (C=O), 1431 (C-N), 1085 (Si-O-Si), 1027 (Si-O-Si), 743 (Si-C).

2.2.6 Synthesis of hepta(phenyl)-POSS-Porphyrin (5-(4-[3-(3-(3,5,7,9,11,13,15-heptaphenyl pentacyclo[9.5.1.1(3,9).1(5,15).1(7,13)]octasiloxane) propyl) ureido]phenyl)-10,15,20-(triphenyl)porphyrin) (Ph-POSS-Porphyrin)

IP-Ph-POSS (22 mg, 0.022 mmol) was dissolved in dry dichloromethane (2 mL) at room temperature. To this solution 5-(4-aminophenyl)-10,15,20-(triphenyl)porphyrin (Porphyrin) (28 mg, 0.045 mmol) and excess DIPEA were added. The final solution was stirred at room temperature for 48 h in a sealed flask. The product was separated using column chromatography on silica gel (Toluene:MeOH ; 80:1). After purification, Ph-POSS-Porphyrin was dried and obtained as a dark powder (Yield = 73% wt).

¹H-NMR (300 MHz, CDCl₃, ppm) δ: 8.83 (m, 8H, Py-H), 8.21 (m, 8H, Ph-H), 7.80-7.74 (m, 25H, Ph-H), 7.44 (m, 7H, Ph-H), 7.37 (m, 14H, Ph-H), 3.34 (t, 2H, -CH₂-N-), 1.62 (m, 2H, -CH₂-), 0.84 (t, 2H, -Si-CH₂-); ²⁹Si-NMR (500 MHz, CDCl₃, ppm) δ: -76.0, -69.1. FTIR (cm⁻¹): 3645 (-NH-CO-NH), 3380 (-NH-), 3062 (C-H, sp²), 2960 (C-H, sp³),

1737 (C=O), 1469 (C-N), 1135 (Si-O-Si), 1109 (Si-O-Si), 742 (Si-C). MALDI-TOF (m/z): $[M]^+$ = 1668.24 observed; $[M]^+$ = 1668.33 calculated.

2.2.7 Synthesis of (tetra-(4-[3-(3-(3,5,7,9,11,13,15-heptaisobutylpentacyclo[9.5.1.1(3,9).1(5,15).1(7,13)]octasiloxane) propyl) ureido] phenyl)-10,15,20-(triphenyl)porphyrin) (tet(IB-POSS)-Porphyrin)

IP-IB-POSS (120 mg, 0.132 mmol) was dissolved in dry dichloromethane (2 mL) at room temperature. To this solution 5,10,15,20-tetra(4-aminophenyl)porphyrin (TAPP) (30 mg, 0.045 mmol) and excess DIPEA were added. The final solution was stirred at room temperature for 48 h in a sealed flask. The product was separated using column chromatography on silica gel (DCM:MeOH ; 5:1). After purification, compound 9 was dried and obtained as a dark red powder (Yield = 83 % wt).

$^1\text{H-NMR}$ (300 MHz, CDCl_3 , ppm) δ : 8.87 (m, 8H, Py-H), 8.05 (m, 8H, PhH), 7.80- 7.70 (m, 8H, Ph-H), 3.34 (t, 8H, $-\text{CH}_2\text{-N-}$), 1.88 (m, 28H, $-\text{CH-}$), 1.76 (m, 8H, $-\text{CH}_2\text{-}$), 0.94 (d, 168H, CH₃), 0.70- 0.60 (m, 64H, $-\text{Si -CH}_2\text{-}$); $^{29}\text{Si-NMR}$ (500 MHz, CDCl_3 , ppm) δ : -65.8. FTIR (cm^{-1}): 3345 ($-\text{NH-CO-NH-}$), 3056 (C-H, sp^2), 2922 (C-H, sp^3), 1436 (C-N), 1088 (Si-O-Si), 1000 (Si-O-Si), 733 (Si-C). MALDI-TOF (m/z): $[M-4\text{H}]^+$ = 4267.39 observed; $[M]^+$ = 4271.46 calculated.

2.2.8 Photophysical Characterization

2.2.8.1 UV-VIS/Fluorescence Spectroscopy

The UV-VIS spectra were recorded from 300 to 800 nm using solutions of the POSS-Porphyrins in THF (6.6 μM) in quartz cuvettes (1 cm path length). Similar

conditions were used for the parent porphyrins (tetraphenylporphyrin (TPP) and Porphyrin). The fluorescence spectra for the POSS-Porphyrins and parent porphyrins were obtained in the same solutions describe above using an excitation wavelength of 520 nm. The fluorescence spectra were recorded from 600 to 800 nm.

The extinction coefficients were obtained using the Beer's Law equation from the linear regression of absorption values vs concentration. For the POSS-Porphyrins, several concentrations in THF ranging from 0.1 to 10 μM were used. Similar conditions were used for the parent porphyrins (Porphyrin and TAPP).

2.2.8.2 Fluorescence Quantum Yield

The fluorescence quantum yields for air-saturated solutions (Φ_F) in THF were determined using the comparative method. Tetraphenylporphyrin (TPP) was used as a reference with a fluorescence quantum yield of 0.12 in benzene.⁴¹ The POSS-Porphyrins concentrations ranged from 0.1 to 10 μM (THF) for the POSS-Porphyrins The excitation wavelength was 520 nm and the excitation and emission slit width were 2 nm. The fluorescence quantum yields were measured according to the comparative method described by the following equation:

$$1) \quad \Phi F_{,Sample} = \Phi F_{,Reference} \cdot \frac{m_{Sample}}{m_{Reference}} \cdot \frac{n^2_{sample}}{n^2_{reference}}$$

where $\Phi F_{,Reference}$ represents the fluorescence quantum yield of a fluorophore reference (TPP), m is the slope of the plotted data relative to the area of the emission peak against the absorption of the fluorophore, whereas n is the refractive index.⁴²

2.2.8.3 Singlet Oxygen Quantum Yield

The $^1\text{O}_2$ quantum yields (Φ_{Δ}) were determined through an indirect method using dimethylantracene (DMA) as the singlet oxygen probe. Several solutions containing DMF were air saturated and prepared with DMA ($50 \mu\text{M}$) and the POSS-Porphyrins or parent porphyrins (TPP and Porphyrin) ($5 \mu\text{M}$). These solutions were covered with aluminum foil to avoid any premature quenching. Quartz cuvettes (1 cm x 1 cm) were filled with 1 mL of the solution and placed in a Spectrofluorophotometer (xenon lamp, Shimadzu RF-5301 PC), and irradiated at 515 nm for 600 s. The absorbance decay of DMA was monitored at 380 nm, which was corrected from light scattering by subtracting the spectra of POSS-Porphyrins. The Φ_{Δ} was calculated using equation (2).

$$2) \quad \Phi_{\Delta,S} = \Phi_{\Delta,R} \cdot \frac{m_S}{m_R} \cdot \frac{1-10^{-absReference}}{1-10^{-absSample}}$$

where $\Phi_{\Delta,S}$ is the singlet oxygen quantum yield of the sample, and m is the slope of the plotted data relative to the area of the emission peak against the absorption of the reference.⁴¹

2.2.9 Cell culture

MDA-MB-231, a human invasive TNBC cell line; was purchased from American Type Culture Collection (ATCC). Breast cancer cells were cultured in RPMI 1640 medium supplemented with 10% FBS, and 1% pen-step at 37 °C with 5% CO₂ atmosphere. The culture media was changed every other day. All cell cultures were maintained in 25 cm² or 75 cm² cell culture flasks and the cells were passaged at 70-80% confluency every 2-4 days.

2.2.10 *In vitro* PDT evaluation

The *in vitro* phototoxicities of 5-(4-aminophenyl)-10,15,20-triphenylporphine (Porphyrin), hepta(isobutyl)-POSS-Porphyrin (IB-POSS-Porphyrin), hepta(phenyl)-POSS-Porphyrin (Ph-POSS-Porphyrin), and tetra-isobutyl-POSS-Porphyrin (tet(IB-POSS)-Porphyrin) were tested by using the MTS assay. For this study, MDA-MB-231 cells were seeded in a 96-well plate at a density of 5×10^3 cells per well in 100 μ L of complete media and incubated at 37 °C in 5% CO₂ atmosphere for 24 h. After removing the cell culture medium, IB-POSS-Porphyrin, Ph-POSS-Porphyrin, and tet(IB-POSS)-Porphyrin solutions (0.01 - 0.5 μ M) were prepared from a 25 μ M stock (in DMSO: 100% vol). After 48 h of incubation in the presence of POSS-Porphyrin materials, the culture media was removed and the cells were washed twice with phosphate buffer solution. MDA-MB-231 cells were illuminated with the red light (630 nm) at a fluence rate of 24.5 mW/cm² for 20 min. Control experiments were maintained in the same conditions, but in the dark for the same interval of time. After irradiation, the media was replaced by fresh media and the cells were allowed to grow for an additional 24 h. To measure the phototoxic and dark toxicity effects the treated MDA-MB-231 cells were subjected to cell viability assay using the Cell Titer 96 Aqueous solution assay. To perform the assay, the cell media was removed and the cells were washed twice with phosphate buffer solution. Fresh media (100 μ L) together with 20 μ L of CellTiter was added into each well and incubated for 2-3 h at 37 °C in 5% CO₂ atmosphere. Cell viability (%) was calculated as follows: $\text{viability} = (A_{\text{sample}}/A_{\text{control}}) \times 100\%$, where A_{sample} and A_{control} denote absorbance values of the sample and control wells measured at 490 nm, respectively. The results are reported as the average \pm SD of three experiments. The EC₅₀ values are determined using

GraphPad Prism (v8.1.2 for macOS, La Jolla California, CA, USA) fitting the viability data to a sigmoidal curve mathematical model.

2.2.11 Flow cytometry

Two plates were prepared with 1×10^5 MDA cells per well in complete RPMI media (2 mL) and incubated at 37° C in 5% CO₂ for 48 hours. The media was removed from each well and solutions of Porphyrin, IB-POSS-Porphyrin and Ph-POSS- Porphyrin in DMSO were prepared with varying concentrations (0.1 and 0.5 μM). The solutions (2 mL) were added to the cells and the plates were incubated at 37° C for 24 hours. The POSS-Porphyrin solutions were removed from the wells and the cells were washed with phosphate buffer solution. Trypsin (300 μL) was added to the cells for 3-5 minutes. Media (500 μL) was added to each well. The contents in each well were mixed and the solutions were transferred to Eppendorf tubes and centrifuged (2.5k RPM, 10 min). The supernatant was discarded and phosphate buffer solution (500 μL) was added to each tube. The solutions were mixed and transferred to flow cytometry tubes the Porphyrin and POSS-Porphyrin internalization was measured using a flow cytometer (BD LSRFortessa). Internalization was calculated using the following equation:

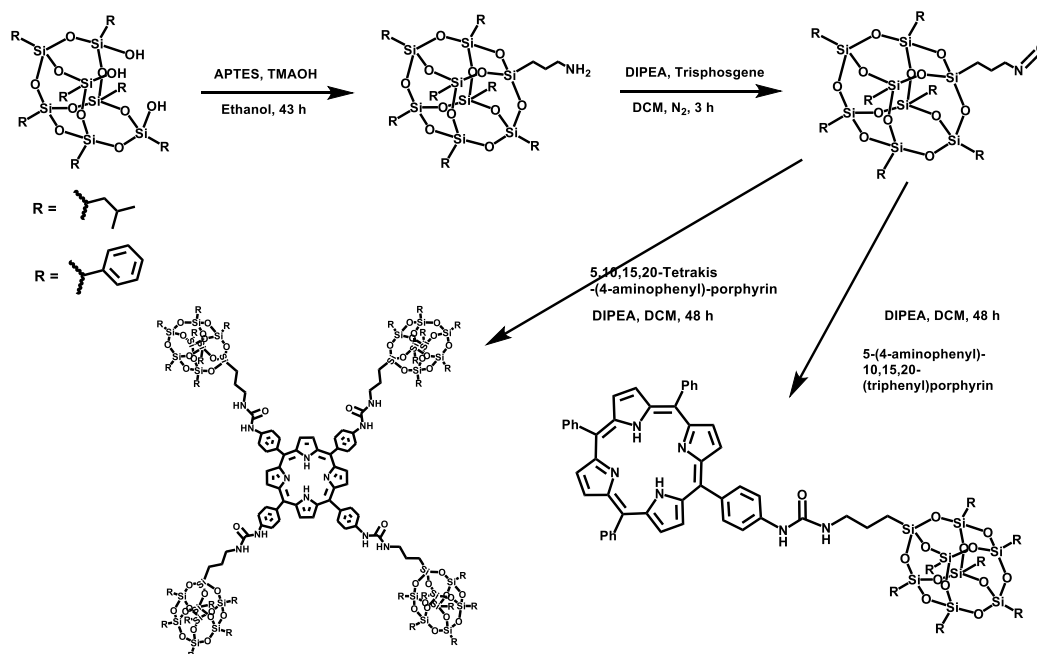
$$3) \quad \text{Relative Fluorescence Intensity (RFI)} = \frac{\text{Sample fitc mean} - \text{neg. control fitc mean}}{\text{neg. control fitc mean}}$$

2.3 Results and Discussion

2.3.1 Synthesis and Characterization of POSS-Porphyrin

The synthesis of the POSS-porphyrin derivatives containing hydrophobic groups, isobutyl (IB-POSS-Porphyrin) and phenyl (Ph-POSS-Porphyrin), was carried out through a multi-step approach (**Scheme 1**). First, commercially available heptaisobutyl- or heptaphenyl-trisilanol POSS was functionalized with aminopropyl trimethoxysilane via a corner capping reaction under basic conditions to afford AP-IB-POSS and AP-Ph-POSS.⁴³ The amine group on those compounds was transformed to an isocyanate group by using triphosgene to produce molecules IP-IB-POSS and IP-Ph-POSS. The successful formation of the cyanate group was shown by the FT-IR stretching vibration at 2273 cm^{-1} . Finally, the mono-aminophenyltriphenyl porphyrin reacted with either compound IP-IB-POSS or IP-Ph-POSS via the formation of a urea bond to afford IB-POSS-Porphyrin or Ph-POSS-Porphyrin, respectively. We also synthesized a tetra-substituted POSS-porphyrin (tet(IB-POSS)-Porphyrin) by reacting an excess of compound IP-IB-POSS with tetra-aminophenylporphyrin following the same reaction as described before. The spectroscopic characterization of IB-, Ph-, and tet(IB)-, POSS-Porphyrin demonstrated the successful synthesis of these compounds. For IB-POSS-Porphyrin, characteristic vibrations in the FT-IR spectra showed the presence of the urea bond at $\sim 1648\text{ cm}^{-1}$ and the Si-O-Si framework at 1084 cm^{-1} which are characteristic of the siloxane cage. Confirmation of the fabrication of IB-POSS-Porphyrin was obtained by ^{29}Si NMR with diagnostic signals in the range of at -67.0, -67.1, -67.3 ppm. In addition, MALDI-TOF mass spectrometry was used to further corroborate the synthesis of the IB-POSS-Porphyrin, showing the expected molecular ions at $[\text{M-H}]^+ = 1527.6$. Ph-POSS-Porphyrin

was also characterized using FT-IR, ^{29}Si NMR, and MALDI-TOF. The urea bond stretch was present at 1655 cm^{-1} in the FT-IR spectra as well as the characteristic siloxane cage Si-O-Si vibrations at 1135 cm^{-1} and 1109 cm^{-1} . In the ^{29}Si NMR, diagnostic signals were present at -69.1 and -76.0 ppm. The molecular ion was present at $[\text{M}]^+ = 1668.2$. Finally, tet(IB-POSS-Porphyrin was characterized using FT-IR and MALDI-TOF. The urea bond vibration was visible at 3345 cm^{-1} with Si-O-Si vibrations at 1088 cm^{-1} and 1000 cm^{-1} . In addition, MALDI-TOF mass spectrometry was used to further corroborate the synthesis of tet(IB-POSS-Porphyrin showing the expected molecular ion $[\text{M}-4\text{H}]^+ = 4267.4$. The complete description for the synthesis and characterization for the intermediate POSS molecules and POSS-Porphyrins, which includes ^1H -NMR, ^{29}Si NMR, FTIR and MALDI-TOF MS, is provided in the experimental section and appendix.



Scheme 1. Synthetic scheme for the synthesis of the POSS-Porphyrins. The synthesis of IB-POSS-Porphyrin and Ph-POSS-Porphyrin follow a similar approach; first, heptaisobutyl- or heptaphenyl-trisilanol POSS was functionalized with aminopropyl trimethoxysilane under basic conditions. Followed by transforming the amine to a cyanate group using triphosgene. Finally, 5-(4-aminophenyl)-10,15,20-(triphenyl)porphyrin reacted with either the isobutyl (IP-IB-POSS) or the phenyl (IP-Ph-POSS) version of POSS cyanate derivative to afford IB-POSS-Porphyrin or Ph-POSS-Porphyrin, respectively. The synthesis of tet(IB-POSS)-Porphyrin was carried out by reacting compound IP-IB-POSS with 5,10,15,20-tetrakis(4-aminophenyl)porphyrin.

2.3.2 Photophysical Characterization

The UV-VIS and fluorescence spectra of the POSS-Porphyrins were measured and compared with the parent porphyrins. Normalized absorption spectra of the POSS-Porphyrin compounds solutions in tetrahydrofuran (THF) showed the typical Soret and Q-bands for porphyrins in the ranges of 410-420, 510-530, 545-565, 585-595 and 645-660 nm (**Figure 6a**). The Soret band wavelengths and the corresponding extinction coefficient values are presented in **Table 1**. The steady-state fluorescence emission spectra with normalized intensities showed two characteristic emission peaks for free-base porphyrins in the range of 650-660 and 715-720 nm (**Figure 6b**). The specific emission wavelengths for the POSS-Porphyrins are provided in **Table 1**. The S- and Q-bands of the POSS-Porphyrins are slightly blue-shifted with respect to their parent porphyrin, Porphyrin or TAPP (**Table A1**). The result is most likely due to the change in the electron-donating effect of the nitrogen substituent in the para (4-phenyl) position when it is chemically transformed from an amine to a urea group as have been demonstrated in the literature.⁴⁴

The fluorescence quantum yields (Φ_F) were determined to indirectly characterize the efficiency with which the POSS-Porphyrin compounds undergo intersystem crossing (ISC) from the excited state to the triplet state, an essential step in ROS generation.⁴⁵ Porphyrin derivatives typically generate low Φ_F indicating that the majority of photons absorbed by porphyrins undergo ISC to the excited triplet. Φ_F in THF for the POSS-Porphyrins were calculated relative to tetraphenylporphyrin (TPP) in benzene. The data shows that the POSS-Porphyrin compounds have lower Φ_F values compared to the parent porphyrins (**Table 1 and A1**), as a possible indication of a more efficient ISC.

The $^1\text{O}_2$ quantum yield (Φ_Δ) of the POSS-porphyrin compounds in dimethyl formamide (DMF) was indirectly determined using 9,10-dimethylanthracene (DMA) as $^1\text{O}_2$ probe. DMA reacts with $^1\text{O}_2$, undergoing a 1,4-cycloaddition that is detected as a decrease in the intensity of the DMA absorption band at 379 nm. The Φ_Δ was calculated relative to the reference TPP ($\Phi_\Delta = 0.62$)⁴⁶ using the slope of the time-dependent decomposition of DMA plots ($\text{Ln}([\text{DMA}_0]/[\text{DMA}])$) versus irradiation times (**Figure A23**), and **Eq 4**.⁴⁶ This pseudofirst-order equation is used under the assumption that there is an excess of singlet oxygen produced compared to the initial concentration of DMA.⁴⁷ The experimental protocol was validated by comparing tetrahydroxy-phenyl-porphyrin and tetraamino-phenyl-porphyrin molecules with known Φ_Δ in DMF, ($\Phi_\Delta = 0.57 \pm 0.03$) and ($\Phi_\Delta = 0.58 \pm 0.04$).⁴⁸ The measured quantum yield values matched the literature values within $\pm 3\%$ error; with a Φ_Δ values of 0.59 ± 0.01 and 0.58 ± 0.01 for tetrahydroxy-phenyl-porphyrin and tetraamino-phenyl-porphyrin molecules, respectively.

$$4) \quad \Phi_{\Delta,S} = \Phi_{\Delta,R} \times \frac{m_S}{m_R} \times \frac{1 - 10^{-Abs_R}}{1 - 10^{-Abs_S}}$$

The Φ_Δ values obtained for POSS-Porphyrins are shown in **Table 1**. Interestingly, all the Φ_Δ values are higher than those corresponding to the parent porphyrins ($p < 0.0001$, **Table A1**). An increase in the Φ_Δ values of 82, 33, and 19%, respectively. The Φ_Δ values for the POSS-Porphyrins follow this trend IB-POSS-Porphyrin > tet(IB-POSS)-Porphyrin > Ph-POSS-Porphyrin. To confirm that this increase is indeed associated to the POSS-Porphyrin molecules and not due to the effect of physical mixture of POSS and the parent porphyrin in solution, the Φ_Δ values for the physical mixture of Ph-POSS-

Porphyrin + Porphyrin were determined. As shown in **Table A1**, the Φ_{Δ} values for the mixtures are lower than the corresponding POSS-Porphyrins. IB-POSS-Porphyrin ($p < 0.0001$), which confirms that the enhancement in Φ_{Δ} is intrinsic to the POSS-Porphyrins. The Φ_{Δ} value could be dependent on several factors: (i) triplet state properties, including quantum yield, lifetime and energy, (ii) the ability of substituents to quench $^1\text{O}_2$ and (iii) the efficiency of energy transfer from the excited triplet state to ground state molecular oxygen.⁴⁹ In the case of porphyrins, the triplet state after irradiation could be inhibited by mutual energy transfer since these molecules favor π -stacking, also known as self-quenching effect.⁵⁰ This effect results in a decline of the ability of porphyrins to generate $^1\text{O}_2$. However, due to the unique 3-D structure of POSS, its steric hindrance suppresses self-quenching of the excited states of porphyrins resulting in the observed enhancement of Φ_{Δ} for POSS-Porphyrins.^{36, 37} It is also relevant to point out that the increase in the Φ_{Δ} values for the POSS-Porphyrins may have an impact on their PDT performance, considering that $^1\text{O}_2$ is one of the main components for the phototoxicity of photosensitizers.

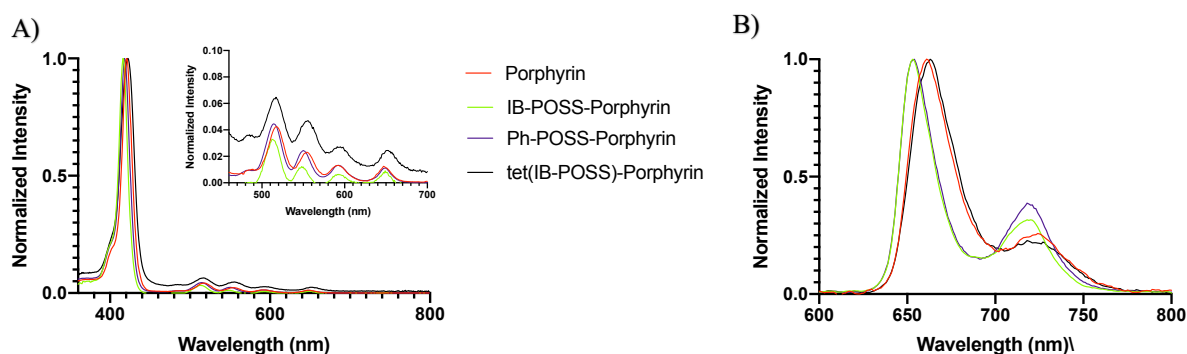


Figure 6. (A) Normalized absorption and (B) emission spectra for 6.6 μM solutions of Porphyrin (red), IB-POSS-Porphyrin (green), Ph-POSS-Porphyrin (purple), and tet(IB-POSS)-Porphyrin (black) in THF. The four Q absorption bands are shown in the inset.

Table 1. Photophysical and photochemical properties of POSS-Porphyrins.

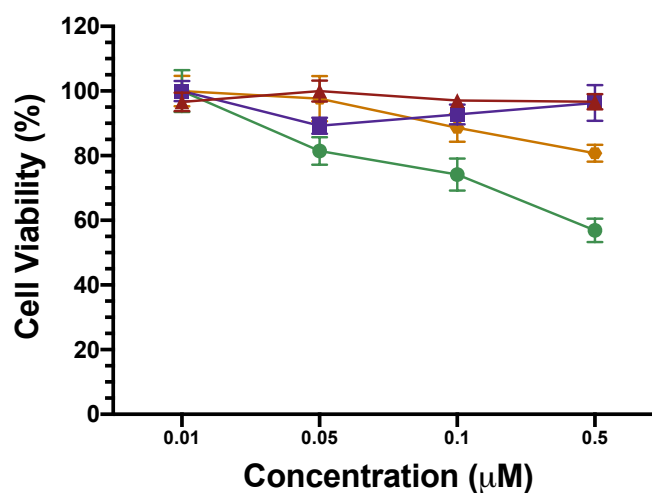
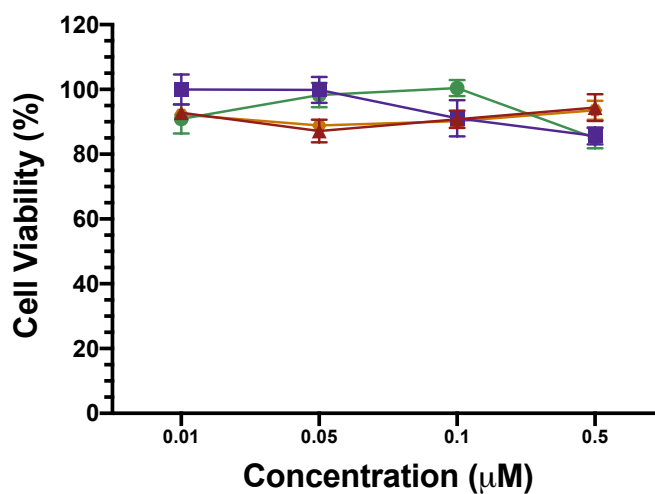
Sample	λ_{Soret} (nm) [$\epsilon \times 10^3$ ($\text{M}^{-1} \text{cm}^{-1}$)] (n=3)	$\lambda_{\text{Emission}}$ (nm)	ϕ_{Δ} (n=3)	ϕ_F (n=3)
Porphyrin	419, 275 \pm 26 (THF)	661, 745	0.45 \pm 0.02	0.21 \pm 0.02 (THF)
IBPOSS-Porphyrin	416, 22.1 \pm 8.3(THF)	653, 720	0.82 \pm 0.01	0.14 \pm 0.01
PhPOSS-Porphyrin	419, 46.2 \pm 9.0 (THF)	653, 719	0.60 \pm 0.02	0.13 \pm 0.01
PhPOSS-Porphyrin+ Porphyrin	N/A	N/A	0.53 \pm 0.01	N/A
tetra(IBPOSS)-Porphyrin	422, 117.3 \pm 34.4 (THF)	663, 719	0.70 \pm 0.01	0.13 \pm 0.02

2.3.3 PDT using POSS-Porphyrin

The phototoxicity of the Porphyrin and POSS-Porphyrin compounds was determined using PDT. The effective concentration needed to result in 50% cell viability (EC_{50}) was used to identify the phototoxic compounds. A smaller EC_{50} in the presence of light corresponds to higher phototoxicity. The porphyrin alone was the only compound determined to be phototoxic with an EC_{50} value of 12 μM (**Figure A24**). The hydrophobic-functionalized POSS-Porphyrin molecules, IB-POSS-Porphyrin, Ph-POSS-Porphyrin, and tet(IB-POSS)-Porphyrin were prepared to a max concentration of 0.5 μM due to their hydrophobicity. An EC_{50} value could not be calculated at this concentration for the hydrophobic molecules (**Figure 7**). Instead, the cell viability was compared at 0.5 μM for all POSS-Porphyrin molecules (**Table 2**). It is evident that IB-POSS-Porphyrin was 20-fold more phototoxic than the Porphyrin alone at this concentration. A comparable phototoxicity is seen when Porphyrin reaches a concentration of 10 μM (**Figure A24**). None of the Porphyrin or POSS-Porphyrin molecules were toxic in the absence of light (**Figure 8**).

Table 2. Porphyrin and POSS-Porphyrin cell viability percentage at 0.5 μM .

Molecule	Cell Viability at 0.5 μM (%)	
	Light	Dark (ctrl)
Porphyrin	97 \pm 2	99 \pm 4
IB-POSS-Porphyrin	57 \pm 4	85 \pm 3
Ph-POSS-Porphyrin	96 \pm 6	86 \pm 3
tet(IB-POSS)-Porphyrin	81 \pm 3	94 \pm 3

**Figure 7.** Phototoxicity of Porphyrin (red), IB-POSS-Porphyrin (green), Ph-POSS-Porphyrin (purple), and tet(IB-POSS)-Porphyrin (orange).**Figure 8.** Cytotoxicity of Porphyrin (red), IB-POSS-Porphyrin (green), Ph-POSS-Porphyrin (purple), and tet(IB-POSS)-Porphyrin (orange).

2.3.4 Flow cytometry

The internalization of the Porphyrin and POSS-Porphyrin molecules in MDA-MB-231 cells was quantified using the relative fluorescence intensity (RFI). Concentrations of 0.1 and 0.5 μM were prepared for all three compounds due to their hydrophobicity. The Porphyrin and IB-POSS-Porphyrin had a RFI of 0.09 ± 0.02 and 0.15 ± 0.02 , respectively, at 0.1 μM and 0.30 ± 0.06 and 0.21 ± 0.06 , respectively, at 0.5 μM (**Figure 9**). Ph-POSS-Porphyrin had an RFI of 1.09 ± 0.11 and 4.02 ± 0.67 at 0.1 and 0.5 μM , respectively (**Figure 9**). The internalization of Ph-POSS-Porphyrin was higher than that of the Porphyrin and IB-POSS-Porphyrin. This data does not support the PDT and singlet oxygen quantum yield experiments. However, it proves that increased internalization does not correspond to increased phototoxicity.

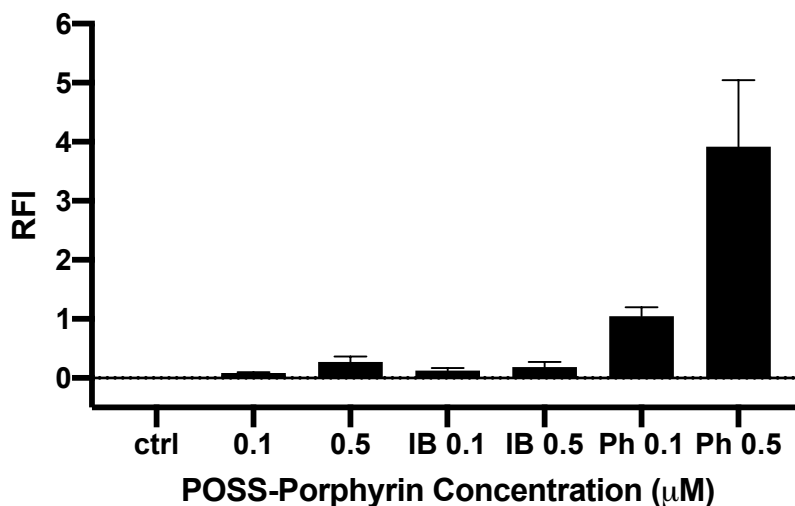


Figure 9. Internalization of POSS-Porphyrin molecules at 0.1 and 0.5 μM (IB is for IB-POSS-Porphyrin and Ph is for Ph-POSS-Porphyrin).

2.4 Conclusions and Future work

A series of polyhedral oligomeric silsesquioxane porphyrin derivatives were synthesized and characterized. The effect of the POSS substituents on the photochemical properties of the POSS-Porphyrins showed that hydrophobic groups produced an increase in the singlet oxygen quantum yield as compared with their parent porphyrins.

The phototoxicity of IB-POSS-Porphyrin, tet(IB-POSS)-Porphyrin, and Ph-POSS-Porphyrin was tested up to 0.5 μM . There was a noticeable impact in phototoxicity from IB-POSS-Porphyrin that was determined to be 20-fold more phototoxic than Porphyrin. This data was supported by the singlet oxygen quantum yield experiments as the IB-POSS-Porphyrin generated the highest amount of singlet oxygen. The trend in phototoxicity from greatest to least: IB-POSS-Porphyrin, tet(IB-POSS)-Porphyrin, Ph-POSS-Porphyrin, Porphyrin, was supported by the singlet oxygen quantum yield experiments. This data was not supported by the internalization studies as Ph-POSS-Porphyrin had the highest RFI corresponding to highest internalization but exhibited no phototoxic effect on the cells. Both IB-POSS-Porphyrin, and Ph-POSS-Porphyrin were determined to have relatively low internalization exhibited a degree of phototoxicity. Despite this, it is proven that the internalization of IB-POSS-Porphyrin has less of an effect than the generation of singlet oxygen leading to the increased phototoxicity of IB-POSS-Porphyrin.

In future work, we will further test the hypothesis by investigating the internalization and subcellular localization of the hydrophobic POSS-Porphyrin molecules. In addition, confocal images of these molecules in mammalian cells will determine if the Porphyrin and POSS-Porphyrin molecules are thoroughly internalized in

the cell or intercalated in the cell membrane. This will aid in the conclusion of the most effective localization of these molecules for increased efficacy for PDT.

Chapter 3: Internalization of POSS in mammalian cells

3.1 Introduction

3.1.1 Mechanism for cellular internalization of molecules

Internalization of molecules occurs through active or passive transport mechanisms. Passive transport can be further broken down into simple diffusion and facilitated diffusion. Energy from the cell is not required for passive transport mechanisms as it is driven by concentration and electrochemical gradients.⁵¹ Small molecules and nonpolar molecules are able to transverse the semi-permeable phospholipid bilayer through simple diffusion while facilitated diffusion is used for larger ions and polar molecules.⁵² Active transport involves cellular energy to encapsulate larger molecules. Most bioactive molecules are internalized through active transport mechanisms. The main active transport process is endocytosis.

3.1.2 Mechanism for cellular internalization of nanoparticles

Nanoparticle (NP) internalization proceeds through an active mechanism, specifically endocytosis.^{53, 54} Through endocytic pathways, NPs are engulfed by the cell membrane and encased in a lipid membrane known as an endosome.⁵⁵ NPs are often trapped in the endosome leading to hydrolytic degradation in the lysosome through the endolysosomal pathway. Inability to escape the endolysosomal pathways reduces the efficacy of drugs.⁵⁶

Endocytosis can be broken into phagocytosis, cell eating reserved for larger materials, and pinocytosis, cellular drinking used for smaller materials ranging in nanometer size.⁵⁷ Macropinocytosis, clathrin- and caveolae-mediated endocytosis, and

clathrin- and caveolae-independent endocytosis are subcategories of pinocytosis.^{55, 57} In both clathrin- and caveolae-mediated endocytosis, proteins are used to encapsulate the material to be internalized.

Mesoporous silica nanoparticle (MSN) have been identified to be internalized through clathrin- and caveolae-mediated mechanisms.⁵³ A study conducted on the effects of surface charge on NP internalization resulted in positively charged NPs more readily internalized through clathrin-dependent pathways while the negatively charged NPs favored uptake by caveolae-dependent pathways.⁵⁸

3.1.3 Mechanism for cellular internalization of POSS

The investigation of POSS internalization is lacking. One study investigated iridium(III)-POSS hybrids for their use as live cell bioimaging reagents.⁵⁹ In addition to confirming the molecules were not cytotoxic, they identified the mechanism of internalization as caveolae-mediated endocytosis.⁵⁹ Another study on luminescent bifunctional POSS molecules involved fluorescein conjugation to an isobutyl POSS which was further functionalized with a carboxylic moiety. The carboxylic functionality was included to anchor organic or inorganic molecules for biomedical applications. The bifunctional POSS molecules were internalized through macropinocytosis, an active mechanism and subcategory of endocytosis.¹⁴

3.1.4 Hypothesis and Aims

We hypothesize that tuning the chemical properties of POSS nanoclusters with different functional groups will impact their internalization. In this project, we investigated the performance of two polyhedral oligomeric silsesquioxane fluorescein

(POSS-fluorescein) compounds for internalization (**Figure 10**). These POSS-fluorescein molecules were rationally designed to contain different functional groups such as alkyl (isobutyl) and aromatic (phenyl). The interactions of these molecules with HeLa cells were investigated to obtain the internalization data.

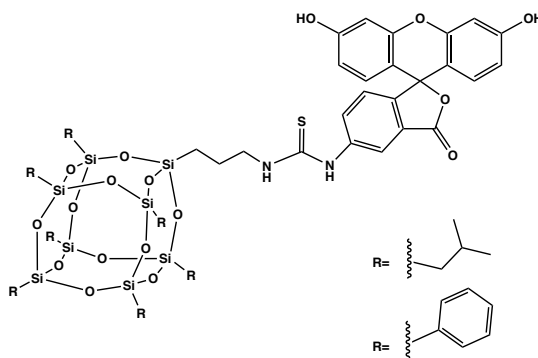


Figure 10. Molecular structure of IB-POSS-fluorescein and Ph-POSS-fluorescein.

3.2 Experiments

3.2.1 Synthesis and characterization of isobutyl-POSS-fluorescein (IB-POSS-fluorescein)

Aminopropyl hepta(isobutyl) POSS (20.0 mg, 0.0197 mmol) and fluorescein (15.6 mg, 0.0401 mmol) were dissolved in THF (4 mL) and stirred at 250 RPM for 24 h. The solvent was removed with a rotary evaporator. Dichloromethane (DCM) was added to remove unreacted fluorescein. The solution was suction filtered and the filtrate was collected. DCM was removed using a rotary evaporator to afford an orange solid and the product was dried under vacuum for 24 h. (Yield = 56 % wt). ^1H NMR (500 MHz, CDCl_3 , ppm) δ : 8.01 (2H, fluorescein-H), 6.97 (1H, fluorescein-H), 3.74 (2H, $-\text{CH}_2\text{-N}$), 1.42 (7H, $-\text{CH}-(\text{CH}_3)_2$), 0.97 (42H, $-\text{CH}_3$), 0.60 (14H, $-\text{CH}_2\text{-Si}$). FTIR (solid, cm^{-1}): 2612-3391 (COOH stretch) 2871-2955 (C-H stretch), 1228 (C=S stretch), 1083 (Si-O-Si stretch). MALDI (m/z): $[\text{M-H}]^- = 1261.8$ observed, $[\text{M}]^+ = 1262.35$ calculated.

3.2.2 Synthesis and characterization of phenyl-POSS-fluorescein (Ph-POSS-fluorescein)

Aminopropyl hepta(phenyl)POSS (48.2 mg, 0.0475 mmol) and fluorescein 38.0 mg, 0.0976 mmol, 2.05 equiv (POSS)) were dissolved in THF (11 mL) and refluxed. Diisopropylethylamine (DIPEA) (24.8 μ L, 0.1424 mmol) was added to the refluxing solution and the reaction was left to reflux at 75 °C for 72h. THF was removed using rotary evaporation. DCM was added to remove fluorescein. The solution was suction filtered and the filtrate was collected. DCM was removed using a rotary evaporator and the orange solid was washed with cold ethanol. The product was collected through centrifugation and dried under vacuum for 24 h. (Yield = 33.1% wt). ^1H NMR (500 MHz, CDCl_3 , ppm) δ : 7.99 (s, 2H, fluorescein-H), 7.72 (m, 14H, Ph-H), 7.60 (s, 1H, fluorescein-H), 7.30-7.48 (m, 25H, Ph-H), 7.19 (s, 1H, fluorescein-H), 6.90 (s, 1H, fluorescein-H), 3.48 (t, 2H, $-\text{CH}_2\text{-N-}$), 2.04 (m, 2H, $-\text{CH}_2\text{-}$), 0.59 (t, 2H, $-\text{Si-CH}_2\text{-}$). FTIR (solid, cm^{-1}): 2589-3627 (COOH stretch), 2925-3074 (sp^3 and sp^2 CH stretch), 1800-1986 (Aromatic overtones), 1255 (C=S stretch), 1089 (Si-O-Si stretch). MALDI (m/z): $[\text{M}+\text{H}]^+ = 1401.0$ observed, $[\text{M}]^+ = 1402.13$ calculated.

3.2.3 Photophysical Characterization

The UV-VIS spectra were recorded from 200 to 800 nm using solutions of POSS-fluorescein in DCM (5 μM) in quartz cuvettes (1 cm path length)(**Figure 11**). The spectra were recorded on a Varian Cary Bio50 UV-VIS absorption spectrophotometer.

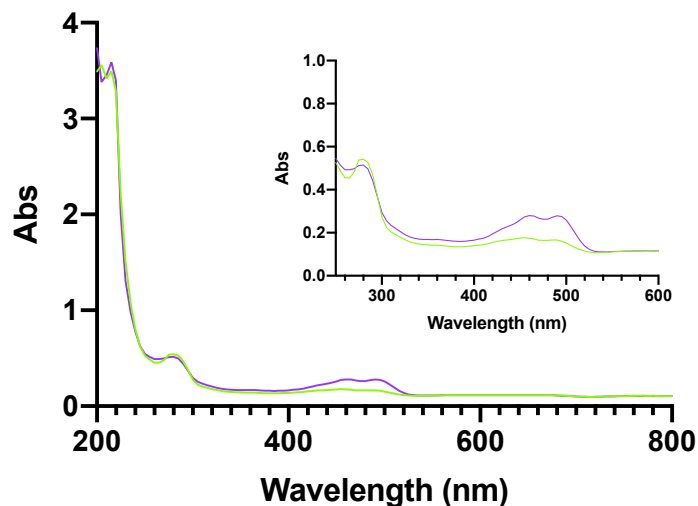


Figure 11. UV-VIS spectrum of IB-POSS-fluorescein and Ph-POSS-fluorescein (green is for IB-POSS-fluorescein and purple is for Ph-POSS-fluorescein).

3.2.4 Toxicity of POSS-fluorescein

The *in vitro* cytotoxicities of fluorescein, hepta(isobutyl)-POSS-fluorescein (IB-POSS-fluorescein) and hepta(phenyl)-POSS-fluorescein (Ph-POSS-fluorescein) were tested by using the MTS assay. For this study, HeLa cells were seeded in a 96-well plate at a density of 5×10^3 cells per well in 100 μL of complete media and incubated at 37 $^{\circ}\text{C}$ in 5% CO_2 atmosphere for 24 h. After removing the cell culture medium, IB-POSS-fluorescein and Ph-POSS-fluorescein solutions (0.01 - 10 μM) were prepared from a 25 μM stock (in DMSO: 100% vol). After 24 h of incubation in the presence of POSS-fluorescein materials, the culture media was removed and the cells were washed once with phosphate buffer solution. To measure the cytotoxic effects, the treated HeLa cells were subjected to cell viability assay using the Cell Titer 96 Aqueous solution assay. Fresh media (100 μL) together with 20 μL of CellTiter was added into each well and incubated for 2-3 h at 37 $^{\circ}\text{C}$ in 5% CO_2 atmosphere. Cell viability (%) was calculated as

follows: $\text{viability} = (A_{\text{sample}}/A_{\text{control}}) \times 100\%$, where A_{sample} and A_{control} denote absorbance values of the sample and control wells measured at 490 nm, respectively. The results are reported as the average \pm SD of three experiments. The EC_{50} values are determined using GraphPad Prism (v8.1.2 for macOS, La Jolla, CA, USA) fitting the viability data to a sigmoidal curve mathematical model.

3.2.5 Temperature-dependent internalization of POSS

Two plates were prepared with 2×10^5 HeLa cells/ well in complete RPMI media (2 mL) and incubated at 37° C in 5% CO₂ for 24 hours. The media was removed from each well and solutions of IB-POSS-fluorescein and Ph-POSS-fluorescein in DMSO were prepared with varying concentrations (5.0 and 10 μM). The solutions (2 mL) were added to the cells and one plate was stored at 4° C, while the other was incubated at 37° C for 4 hours. The IB-POSS-fluorescein and Ph-POSS-fluorescein solutions were removed from the wells and the cells were washed with PBS. Trypsin (300 μL) was added to the cells for 3-5 minutes. Media (500 μL) was added to each well. The contents in each well were mixed and the solutions were transferred to Eppendorf tubes and centrifuged (2.5k RPM, 10 min). The supernatant was discarded and PBS (400 μL) was added to each tube. The solutions were mixed and transferred to flow cytometry tubes and trypan blue (200 μL) was added. The POSS-fluorescein internalization was measured using a flow cytometer. Internalization was calculated using equation 3.

$$3) \quad \text{Relative Fluorescence Intensity (RFI)} = \frac{\text{Sample fitc mean} - \text{neg. control fitc mean}}{\text{neg. control fitc mean}}$$

3.3 Results and Discussion

3.3.1 Synthesis and characterization of POSS-fluorescein

Hepta(isobutyl)-POSS-fluorescein (IB-POSS-fluorescein) was synthesized through the conjugation of aminopropyl-isobutyl-POSS (AP-IB-POSS) to fluorescein via the formation of a thiourea bond. AP-IB-POSS was obtained via a corner capping reaction of previously purchased heptaisobutyl-trisilanol-POSS, with aminopropyltriethoxy silane (APTES) in the presence of tetramethylammonium hydroxide (TMAOH). The final product was characterized using ^1H , ^{13}C and ^{29}Si NMR, FTIR and MALDI-TOF as discussed in chapter 2. Following this, the fluorescein was conjugated to the POSS at room temperature. The final product was characterized using FTIR and MALDI-TOF. MALDI-TOF was used to further confirm the product, showing an observed mass of 1261.8 m/z. Moreover, the FT-IR has a stretching vibration corresponding to a thioketone bond at 1228 cm^{-1} for IB-POSS-fluorescein confirming a successful POSS-fluorescein conjugation.

Hepta(phenyl)-POSS-fluorescein (Ph-POSS-fluorescein) was obtained through the conjugation of aminopropyl-phenyl-POSS (AP-Ph-POSS) to fluorescein via the formation of a urea bond. AP-Ph-POSS was previously synthesized via a corner capping reaction of previously purchased heptaphenyl-trisilanol-POSS, with aminopropyltriethoxy silane (APTES) in the presence of tetramethylammonium hydroxide (TMAOH) in slightly harsher conditions as compared to AP-IB-POSS. The final product was characterized using ^1H , ^{13}C and ^{29}Si NMR, FTIR and MALDI-TOF as discussed in chapter 2.⁶⁰ The reaction performed to conjugate the POSS to fluorescein was completed under reflux under basic conditions. The final product was characterized using FTIR and

MALDI-TOF. MALDI-TOF was used to further confirm the product, showing an observed mass of 1401.0 m/z. Finally, the thioketone stretch was observed in the FTIR spectrum at 1255 cm^{-1} , confirming the successful conjugation of Ph-POSS-fluorescein.

3.3.2 Photophysical Properties of POSS-fluorescein

The UV-VIS spectra of the POSS-fluorescein molecules were measured.

Normalized absorption spectra of the POSS-fluorescein compounds solutions in dimethyl sulfoxide (DMSO) showed the typical absorbance peak from 460-500 nm. The fluorescein absorbance peak appears near 490 nm. This dictated the laser used for the internalization experiments.

3.3.3 Toxicity of POSS-fluorescein

The cytotoxic effects of IB-POSS-fluorescein and Ph-POSS-fluorescein were tested in HeLa cells. DMSO was used to solubilize the molecules before preparing the 0.01-10 μM solutions in media (<1% DMSO). Neither of the POSS-fluorescein compounds were determined to be cytotoxic at concentrations 0.01-10 μM , as expected (**Figure 12**). Both POSS molecules and fluorescein are known to have minimal toxicity in mammalian cells at low concentrations.¹⁴ This is ideal as the influence of POSS functionalization as a directing agent is of interest. As proposed in our hypothesis, we predict the functional groups on the POSS moiety will influence the internalization and cellular localization which can be used in therapeutic studies by conjugating POSS to a therapeutic. The lack of toxicity from fluorescein was also expected due to it being a known labeling dye.

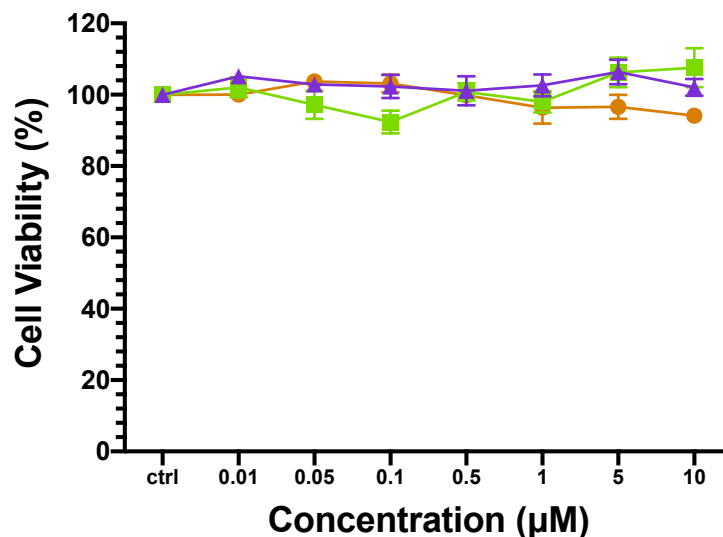


Figure 12. Cytotoxicity of POSS-fluorescein compounds (green is for IB-POSS-fluorescein, purple is for Ph-POSS-fluorescein, and orange is for fluorescein).

3.3.4 Mechanism of cellular internalization of POSS-fluorescein

Molecules can be internalized through active transport mechanisms that require energy or passive transport mechanisms through which energy is not required. Temperature-dependent internalization studies are used to identify the method as active or passive.

Cells are seeded and inoculated 24 h later with the molecules of interest after which they are incubated at 4° C or 37° C. Reducing the temperature restricts cell membrane transport functions that require energy due to membrane rigidity.⁶¹ To identify which mechanism POSS-fluorescein molecules are internalized through, temperature-dependent internalization intensities were compared between IB-POSS- fluorescein and Ph-POSS- fluorescein (**Figure 13**). The solutions were prepared in DMSO at 5 and 10 µM. Both IB-POSS-fluorescein and Ph-POSS-fluorescein showed a higher RFI corresponding to

higher internalization when incubated in 37° C confirming an energy-dependent internalization mechanism.

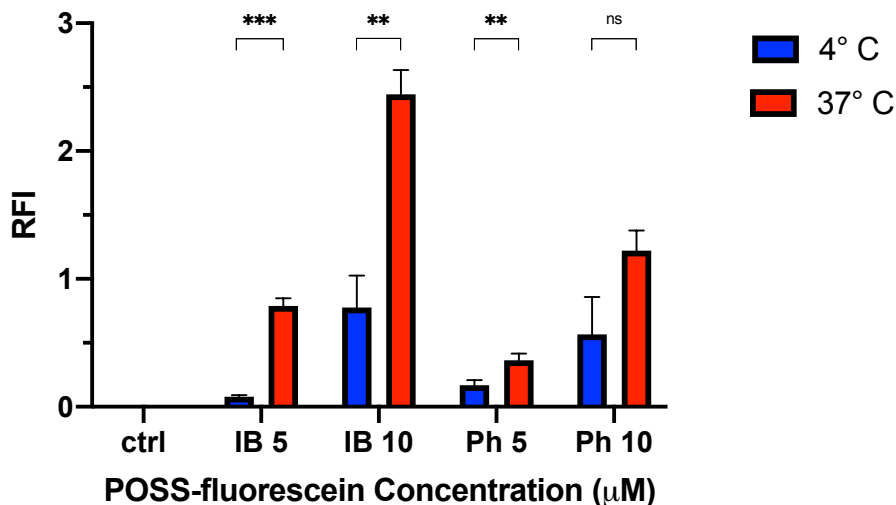


Figure 13. Temperature-dependent internalization of IB-POSS-fluorescein and Ph-POSS-fluorescein (5 and 10 µM in DMSO) (blue is for 4° C and red is for 37° C). *** $p \leq 0.001$, ** $p \leq 0.01$, * $p \leq 0.05$, and ns $p > 0.05$.

3.4 Conclusions and Future work

Hydrophobic-functionalized POSS-fluorescein molecules were synthesized through a covalent conjugation of AP-IB-POSS or AP-Ph-POSS and fluorescein isothiocyanate. The molecules were characterized with ^1H NMR, IR, and MALDI-TOF to confirm the structures. The C=S stretch in the IR confirmed the successful formation of the thiourea bond which conjugated the POSS and fluorescein molecules. The molecular ion was identified in MALDI-TOF.

Following the synthesis and characterization of the POSS-fluorescein molecules, the cytotoxicity studies proved that the molecules have minimal toxicity and the temperature-dependent internalization studies determined an active method of internalization. Both IB-POSS-fluorescein and Ph-POSS-fluorescein were internalized at

a higher rate when incubated in 37° C as opposed to 4° C. The membrane rigidity that occurs with temperature reduction did not allow for internalization of these hydrophobic molecules.

In the future, we plan to further investigate the specific energy-dependent mechanism of internalization as macropinocytosis, clathrin- or caveolae-mediated endocytosis, or clathrin- or caveolae-independent endocytosis. This will be evaluated using inhibitors specific to the endocytic pathways. For macropinocytosis, wortmannin is the inhibiting agent and chlorpromazine and genistein are the inhibiting agents clathrin- and caveolae-mediated endocytosis, respectively.⁵³ Furthermore, we will obtain confocal images of the molecules to corroborate the intracellular colocalization of the POSS-fluorescein molecules.

CHAPTER 4: CONCLUSIONS AND FUTURE WORK

Polyhedral Oligomeric Silsesquioxane (POSS) molecules are increasingly being studied for their use in biomedical applications. The low toxicity and high biocompatibility of these molecules make them ideal candidates as drug carriers. As hybrid organic-inorganic composites, POSS compounds have the ability to exploit the advantages of organic and inorganic materials, while avoiding the downsides. POSS molecules are also known by their exceptional biodegradability and mechanical properties due to the Si-O-Si bonds that comprise the core. Taking advantage of the properties of POSS molecules, we can use them to improve the performance of techniques such as photodynamic therapy (PDT) and drug delivery.

In this thesis, we investigated the influence of hydrophobic-functionalized POSS molecules on PDT and their internalization by mammalian cells. Specifically, we used an aliphatic group (isobutyl), an aromatic group (phenyl), and a tetra(POSS) derivative to test steric effects. The functionalization of the porphyrin moiety with IB-POSS-Porphyrin and tet(POSS)-Porphyrin had an effect on the photophysical characteristics as well as the phototoxicity. IB-POSS-Porphyrin had the highest singlet oxygen quantum yield; and therefore, it was the most phototoxic. Since singlet oxygen production is ideal for PDT to be effective, the phototoxic effects seen from IB-POSS-Porphyrin are supported.

The ability to add a reactive group to POSS molecules allows for multifunctionality. In addition to conjugating hydrophobic POSS moieties to porphyrins, we were able to conjugate them to a fluorescent dye, fluorescein, to study internalization. Internalization studies allow for a deeper understanding of how the molecules interact with mammalian cells. The method of internalization was determined to be energy-

dependent, which indicates that cells use an active transport mechanism such as macropinocytosis, clathrin- or caveolae-mediated endocytosis, or clathrin- or caveolae-independent endocytosis. Future work will include studying the specific mechanism of internalization more in depth using inhibitors as well as identifying the intracellular localization of these molecules. Furthermore, conducting the photophysical, PDT, and internalization studies of hydrophilic POSS-Porphyrin, which are currently in progress, and POSS-fluorescein derivatives will allow for a more comprehensive study on how substituents influence PDT effectiveness and internalization.

REFERENCES

1. Patra, J. K.; Das, G.; Fraceto, L. F.; Campos, E. V. R.; Rodriguez-Torres, M. d. P.; Acosta-Torres, L. S.; Diaz-Torres, L. A.; Grillo, R.; Swamy, M. K.; Sharma, S.; Habtemariam, S.; Shin, H.-S., Nano based drug delivery systems: recent developments and future prospects. *Journal of Nanobiotechnology* **2018**, *16* (1), 71.
2. Jiang, W.; Kim, B. Y.; Rutka, J. T.; Chan, W. C., Advances and challenges of nanotechnology-based drug delivery systems. *Expert opinion on drug delivery* **2007**, *4* (6), 621-33.
3. Wen, H.; Jung, H.; Li, X., Drug Delivery Approaches in Addressing Clinical Pharmacology-Related Issues: Opportunities and Challenges. *The AAPS journal* **2015**, *17* (6), 1327-1340.
4. Mitragotri, S.; Burke, P. A.; Langer, R., Overcoming the challenges in administering biopharmaceuticals: formulation and delivery strategies. *Nat Rev Drug Discov* **2014**, *13* (9), 655-672.
5. Paul, W.; Sharma, C. P., 8 - Inorganic nanoparticles for targeted drug delivery. In *Biointegration of Medical Implant Materials*, Sharma, C. P., Ed. Woodhead Publishing: 2010; pp 204-235.
6. Zhang, Y.-N.; Poon, W.; Tavares, A. J.; McGilvray, I. D.; Chan, W. C. W., Nanoparticle–liver interactions: Cellular uptake and hepatobiliary elimination. *Journal of Controlled Release* **2016**, *240*, 332-348.
7. Zhang, Q.; Yang, M.; Zhu, Y.; Mao, C., Metallic Nanoclusters for Cancer Imaging and Therapy. *Curr Med Chem* **2018**, *25* (12), 1379-1396.
8. Zhang, X.-D.; Wu, D.; Shen, X.; Liu, P.-X.; Fan, F.-Y.; Fan, S.-J., In vivo renal clearance, biodistribution, toxicity of gold nanoclusters. *Biomaterials* **2012**, *33* (18), 4628-4638.
9. Song, X. R.; Goswami, N.; Yang, H. H.; Xie, J., Functionalization of metal nanoclusters for biomedical applications. *The Analyst* **2016**, *141* (11), 3126-40.
10. Zhou, F.; Feng, B.; Yu, H.; Wang, D.; Wang, T.; Liu, J.; Meng, Q.; Wang, S.; Zhang, P.; Zhang, Z.; Li, Y., Cisplatin Prodrug-Conjugated Gold Nanocluster for Fluorescence Imaging and Targeted Therapy of the Breast Cancer. *Theranostics* **2016**, *6* (5), 679-687.

11. Yu, Y.; Geng, J.; Ong, E. Y. X.; Chellappan, V.; Tan, Y. N., Bovine Serum Albumin Protein-Templated Silver Nanocluster (BSA-Ag13): An Effective Singlet Oxygen Generator for Photodynamic Cancer Therapy. *Advanced Healthcare Materials* **2016**, *5* (19), 2528-2535.
12. Njuguna, J.; Ansari, F.; Sachse, S.; Zhu, H.; Rodriguez, V. M., 1 - Nanomaterials, nanofillers, and nanocomposites: types and properties. In *Health and Environmental Safety of Nanomaterials*, Njuguna, J.; Pielichowski, K.; Zhu, H., Eds. Woodhead Publishing: 2014; pp 3-27.
13. Fabritz, S.; Hörner, S.; Avrutina, O.; Kolmar, H., Bioconjugation on cube-octameric silsesquioxanes. *Organic & Biomolecular Chemistry* **2013**, *11* (14), 2224-2236.
14. Olivero, F.; Renò, F.; Carniato, F.; Rizzi, M.; Cannas, M.; Marchese, L., A novel luminescent bifunctional POSS as a molecular platform for biomedical applications. *Dalton Transactions* **2012**, *41* (25), 7467-7473.
15. Kannan, R. Y.; Salacinski, H. J.; Butler, P. E.; Seifalian, A. M., Polyhedral Oligomeric Silsesquioxane Nanocomposites: The Next Generation Material for Biomedical Applications. *Accounts of Chemical Research* **2005**, *38* (11), 879-884.
16. Oseni, A. O.; Butler, P. E.; Seifalian, A. M., The application of POSS nanostructures in cartilage tissue engineering: the chondrocyte response to nanoscale geometry. *Journal of tissue engineering and regenerative medicine* **2015**, *9* (11), E27-38.
17. Tanaka, K.; Chujo, Y., Advanced functional materials based on polyhedral oligomeric silsesquioxane (POSS). *Journal of Materials Chemistry* **2012**, *22* (5), 1733-1746.
18. Ding, D.; Pu, K. Y.; Li, K.; Liu, B., Conjugated oligoelectrolyte-polyhedral oligomeric silsesquioxane loaded pH-responsive nanoparticles for targeted fluorescence imaging of cancer cell nucleus. *Chemical communications (Cambridge, England)* **2011**, *47* (35), 9837-9.
19. McCusker, C.; Carroll, J. B.; Rotello, V. M., Cationic polyhedral oligomeric silsesquioxane (POSS) units as carriers for drug delivery processes. *Chemical Communications* **2005**, (8), 996-998.
20. McCusker, C.; Carroll, J. B.; Rotello, V. M., Cationic polyhedral oligomeric silsesquioxane (POSS) units as carriers for drug delivery processes. *Chemical communications (Cambridge, England)* **2005**, (8), 996-8.
21. Zhang, W.-B.; Li, Y.; Li, X.; Dong, X.; Yu, X.; Wang, C.-L.; Wesdemiotis, C.; Quirk, R. P.; Cheng, S. Z. D., Synthesis of Shape Amphiphiles Based on Functional

Polyhedral Oligomeric Silsesquioxane End-Capped Poly(L-Lactide) with Diverse Head Surface Chemistry. *Macromolecules* **2011**, *44* (8), 2589-2596.

22. Yuan, H.; Luo, K.; Lai, Y.; Pu, Y.; He, B.; Wang, G.; Wu, Y.; Gu, Z., A Novel Poly(L-glutamic acid) Dendrimer Based Drug Delivery System with Both pH-Sensitive and Targeting Functions. *Molecular Pharmaceutics* **2010**, *7* (4), 953-962.

23. Calzoni, E.; Cesaretti, A.; Polchi, A.; Di Michele, A.; Tancini, B.; Emiliani, C., Biocompatible Polymer Nanoparticles for Drug Delivery Applications in Cancer and Neurodegenerative Disorder Therapies. *Journal of functional biomaterials* **2019**, *10* (1), 4.

24. Plaetzer, K.; Krammer, B.; Berlanda, J.; Berr, F.; Kiesslich, T., Photophysics and photochemistry of photodynamic therapy: fundamental aspects. *Lasers in Medical Science* **2009**, *24* (2), 259-268.

25. Mustafa, F. H.; Jaafar, M. S.; Ismail, A. H.; Houssein, H. A. A. In *The effect of laser wavelength in photodynamic therapy and phototherapy for superficial skin diseases*, 2011 IEEE International Conference on Imaging Systems and Techniques, 17-18 May 2011; 2011; pp 232-236.

26. Nowis, D.; Makowski, M.; Stoklosa, T.; Legat, M.; Issat, T.; Golab, J., Direct tumor damage mechanisms of photodynamic therapy. *Acta biochimica Polonica* **2005**, *52* (2), 339-52.

27. Obaid, G.; Broekgaarden, M.; Bulin, A.-L.; Huang, H.-C.; Kuriakose, J.; Liu, J.; Hasan, T., Photonanomedicine: a convergence of photodynamic therapy and nanotechnology. *Nanoscale* **2016**, *8* (25), 12471-12503.

28. Dai, T.; Fuchs, B.; Coleman, J.; Prates, R.; Astrakas, C.; G St Denis, T.; Ribeiro, M.; Mylonakis, E.; Hamblin, M.; Tegos, G., *Concepts and Principles of Photodynamic Therapy as an Alternative Antifungal Discovery Platform*. 2012; Vol. 3, p 120.

29. Abrahamse, H.; Hamblin, M. R., New photosensitizers for photodynamic therapy. *Biochem J* **2016**, *473* (4), 347-364.

30. Dolmans, D. E. J. G. J.; Fukumura, D.; Jain, R. K., Photodynamic therapy for cancer. *Nature Reviews Cancer* **2003**, *3* (5), 380-387.

31. Lin, Y.; Zhou, T.; Bai, R.; Xie, Y., Chemical approaches for the enhancement of porphyrin skeleton-based photodynamic therapy. *Journal of Enzyme Inhibition and Medicinal Chemistry* **2020**, *35* (1), 1080-1099.

32. Yano, S.; Hirohara, S.; Obata, M.; Hagiya, Y.; Ogura, S.-i.; Ikeda, A.; Kataoka, H.; Tanaka, M.; Joh, T., Current states and future views in photodynamic therapy. *Journal of Photochemistry and Photobiology C: Photochemistry Reviews* **2011**, *12* (1), 46-67.
33. Celli, J. P.; Spring, B. Q.; Rizvi, I.; Evans, C. L.; Samkoe, K. S.; Verma, S.; Pogue, B. W.; Hasan, T., Imaging and photodynamic therapy: mechanisms, monitoring, and optimization. *Chemical reviews* **2010**, *110* (5), 2795-2838.
34. Zhu, Y.-X.; Jia, H.-R.; Chen, Z.; Wu, F.-G., Photosensitizer (PS)/polyhedral oligomeric silsesquioxane (POSS)-crosslinked nanohybrids for enhanced imaging-guided photodynamic cancer therapy. *Nanoscale* **2017**, *9* (35), 12874-12884.
35. Kim, Y. J.; Lee, H. I.; Kim, J. K.; Kim, C. H.; Kim, Y. J., Peptide 18-4/chlorin e6-conjugated polyhedral oligomeric silsesquioxane nanoparticles for targeted photodynamic therapy of breast cancer. *Colloids and surfaces. B, Biointerfaces* **2020**, *189*, 110829.
36. Jin, J.; Zhu, Y.; Zhang, Z.; Zhang, W., Enhancing the Efficacy of Photodynamic Therapy through a Porphyrin/POSS Alternating Copolymer. *Angewandte Chemie (International ed. in English)* **2018**, *57* (50), 16354-16358.
37. Chen, J.; Xu, Y.; Gao, Y.; Yang, D.; Wang, F.; Zhang, L.; Bao, B.; Wang, L., Nanoscale Organic-Inorganic Hybrid Photosensitizers for Highly Effective Photodynamic Cancer Therapy. *ACS Applied Materials & Interfaces* **2018**, *10* (1), 248-255.
38. Zhou, J.; Zhao, Y.; Yu, K.; Zhou, X.; Xie, X., Synthesis, thermal stability and photoresponsive behaviors of azobenzene-tethered polyhedral oligomeric silsesquioxanes. *New Journal of Chemistry* **2011**, *35* (12), 2781-2792.
39. York, M.; Evans, R. A., The use of polyhedral oligomeric silsesquioxane (POSS) as a soluble support for organic synthesis: A case study with a POSS-bound isocyanate scavenger reagent. *Tetrahedron Letters* **2010**, *51* (35), 4677-4680.
40. Wheeler, P. A.; Fu, B. X.; Lichtenhan, J. D.; Weitao, J.; Mathias, L. J., Incorporation of metallic POSS, POSS copolymers, and new functionalized POSS compounds into commercial dental resins. *Journal of Applied Polymer Science* **2006**, *102* (3), 2856-2862.
41. Angeli, N. G.; Lagorio, M. G.; San Román, E. A.; Dicio, L. E., Meso-substituted cationic porphyrins of biological interest. Photophysical and physicochemical properties in solution and bound to liposomes. *Photochemistry and photobiology* **2000**, *72* (1), 49-56.

42. Marin, D. M.; Payerpaj, S.; Collier, G. S.; Ortiz, A. L.; Singh, G.; Jones, M.; Walter, M. G., Efficient intersystem crossing using singly halogenated carbomethoxyphenyl porphyrins measured using delayed fluorescence, chemical quenching, and singlet oxygen emission. *Physical Chemistry Chemical Physics* **2015**, *17* (43), 29090-29096.
43. Cordes, D. B.; Lickiss, P. D.; Rataboul, F., Recent Developments in the Chemistry of Cubic Polyhedral Oligosilsesquioxanes. *Chemical Reviews* **2010**, *110* (4), 2081-2173.
44. Giovanelli, L.; Lee, H. L.; Lacaze-Dufaure, C.; Koudia, M.; Clair, S.; Lin, Y. P.; Ksari, Y.; Themlin, J. M.; Abel, M.; Cafolla, A. A., Electronic structure of tetra(4-aminophenyl)porphyrin studied by photoemission, UV-Vis spectroscopy and density functional theory. *Journal of Electron Spectroscopy and Related Phenomena* **2017**, *218*, 40-45.
45. Hurst, A. N.; Scarbrough, B.; Saleh, R.; Hovey, J.; Ari, F.; Goyal, S.; Chi, R. J.; Troutman, J. M.; Vivero-Escoto, J. L., Influence of Cationic meso-Substituted Porphyrins on the Antimicrobial Photodynamic Efficacy and Cell Membrane Interaction in *Escherichia coli*. *International journal of molecular sciences* **2019**, *20* (1).
46. Caminos, D.; Spesia, M.; Durantini, E., Photodynamic inactivation of *Escherichia coli* by novel meso-substituted porphyrins by 4-(3-N,N,N-trimethylammoniumpropoxy)phenyl and 4-(trifluoromethyl)phenyl groups. *Photochemical & photobiological sciences : Official journal of the European Photochemistry Association and the European Society for Photobiology* **2006**, *5*, 56-65.
47. Albiter, E.; Alfaro, S.; Valenzuela, M. A., Photosensitized oxidation of 9,10-dimethylanthracene with singlet oxygen by using a safranin O/silica composite under visible light. *Photochemical & Photobiological Sciences* **2015**, *14* (3), 597-602.
48. Ormond, A. B.; Freeman, H., Effects of substituents on the photophysical properties of symmetrical porphyrins. *Dyes and Pigments* **2013**, *96*, 440-448.
49. van Leeuwen, M.; Beeby, A.; Fernandes, I.; Ashworth, S. H., The photochemistry and photophysics of a series of alpha octa(alkyl-substituted) silicon, zinc and palladium phthalocyanines. *Photochemical & Photobiological Sciences* **2014**, *13* (1), 62-69.
50. Engelmann, F. M.; Mayer, I.; Gabrielli, D. S.; Toma, H. E.; Kowaltowski, A. J.; Araki, K.; Baptista, M. S., Interaction of cationic meso-porphyrins with liposomes, mitochondria and erythrocytes. *Journal of bioenergetics and biomembranes* **2007**, *39* (2), 175-85.
51. Yang, N. J.; Hinner, M. J., Getting across the cell membrane: an overview for small molecules, peptides, and proteins. *Methods Mol Biol* **2015**, *1266*, 29-53.

52. Kou, L.; Sun, J.; Zhai, Y.; He, Z., The endocytosis and intracellular fate of nanomedicines: Implication for rational design. *Asian Journal of Pharmaceutical Sciences* **2013**, *8* (1), 1-10.
53. Walker, W. A.; Tarannum, M.; Vivero-Escoto, J. L., Cellular endocytosis and trafficking of cholera toxin B-modified mesoporous silica nanoparticles. *Journal of Materials Chemistry B* **2016**, *4* (7), 1254-1262.
54. Mosquera, J.; García, I.; Liz-Marzán, L. M., Cellular Uptake of Nanoparticles versus Small Molecules: A Matter of Size. *Accounts of Chemical Research* **2018**, *51* (9), 2305-2313.
55. Doherty, G. J.; McMahon, H. T., Mechanisms of endocytosis. *Annual review of biochemistry* **2009**, *78*, 857-902.
56. Slowing, I.; Trewyn, B. G.; Lin, V. S. Y., Effect of Surface Functionalization of MCM-41-Type Mesoporous Silica Nanoparticles on the Endocytosis by Human Cancer Cells. *Journal of the American Chemical Society* **2006**, *128* (46), 14792-14793.
57. Foroozandeh, P.; Aziz, A. A., Insight into Cellular Uptake and Intracellular Trafficking of Nanoparticles. *Nanoscale Res Lett* **2018**, *13* (1), 339-339.
58. Bannunah, A. M.; Vllasaliu, D.; Lord, J.; Stolnik, S., Mechanisms of Nanoparticle Internalization and Transport Across an Intestinal Epithelial Cell Model: Effect of Size and Surface Charge. *Molecular Pharmaceutics* **2014**, *11* (12), 4363-4373.
59. Zhu, J. H.; Tang, B. Z.; Lo, K. K., Luminescent Molecular Octopuses with a Polyhedral Oligomeric Silsesquioxane (POSS) Core and Iridium(III) Polypyridine Arms: Synthesis, Aggregation Induced Emission, Cellular Uptake, and Bioimaging Studies. *Chemistry (Weinheim an der Bergstrasse, Germany)* **2019**, *25* (45), 10633-10641.
60. Matsumoto, J.; Matsumoto, T.; Senda, Y.; Shiragami, T.; Yasuda, M., Preparation and characterization of porphyrin chromophores immobilized on micro-silica gel beads. *Journal of Photochemistry and Photobiology A-chemistry - J PHOTOCHEM PHOTOBIOLOG A-CHEM* **2008**, *197*, 101-109.
61. Behzadi, S.; Serpooshan, V.; Tao, W.; Hamaly, M. A.; Alkawareek, M. Y.; Dreaden, E. C.; Brown, D.; Alkilany, A. M.; Farokhzad, O. C.; Mahmoudi, M., Cellular uptake of nanoparticles: journey inside the cell. *Chem Soc Rev* **2017**, *46* (14), 4218-4244.

APPENDIX

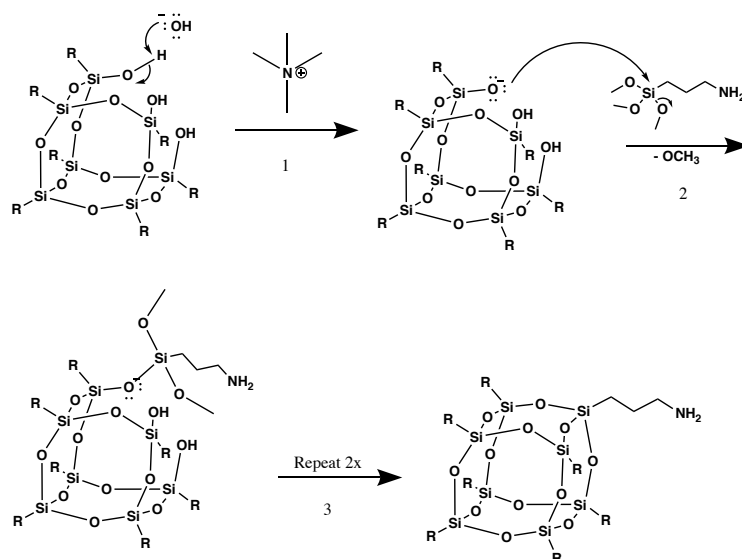


Figure A1. Mechanism of corner capping reaction of a partially condensed hydrophobic-functionalized trisilanol POSS under TMAH with a reactive aminopropyl moiety.

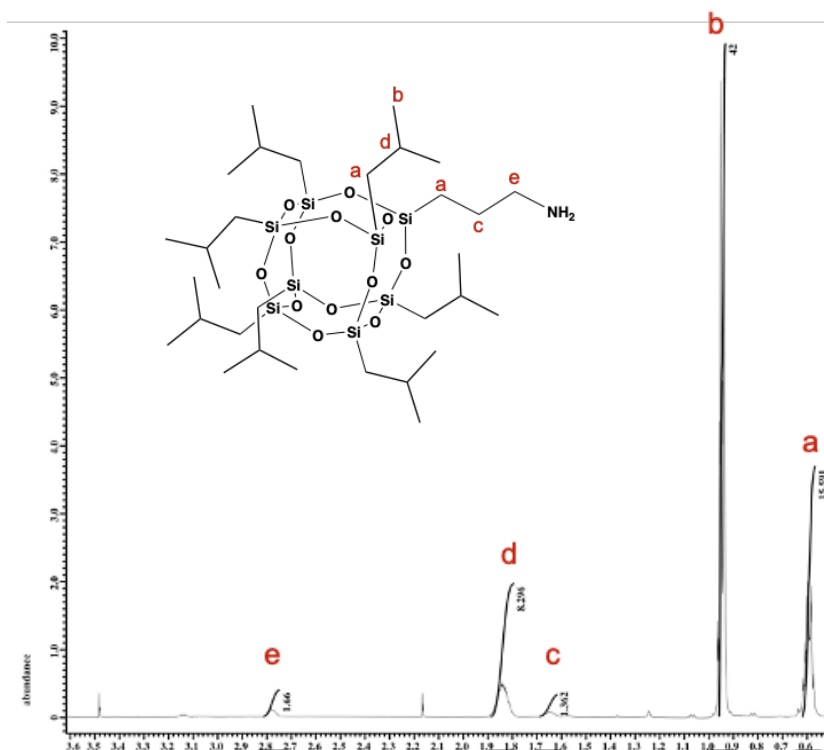


Figure A2. ^1H NMR of AP-IB-POSS. (300 MHz, CDCl_3 , ppm) δ : 2.78 (t, 2H, $-\text{CH}_2-\text{N}-$), 1.85 (m, 7H, $-\text{CH}-$), 1.66 (m, 2H, $-\text{CH}_2-$), 0.94 (d, 42H, CH_3), 0.60 (m, 16H, $-\text{Si}-\text{CH}_2-$).

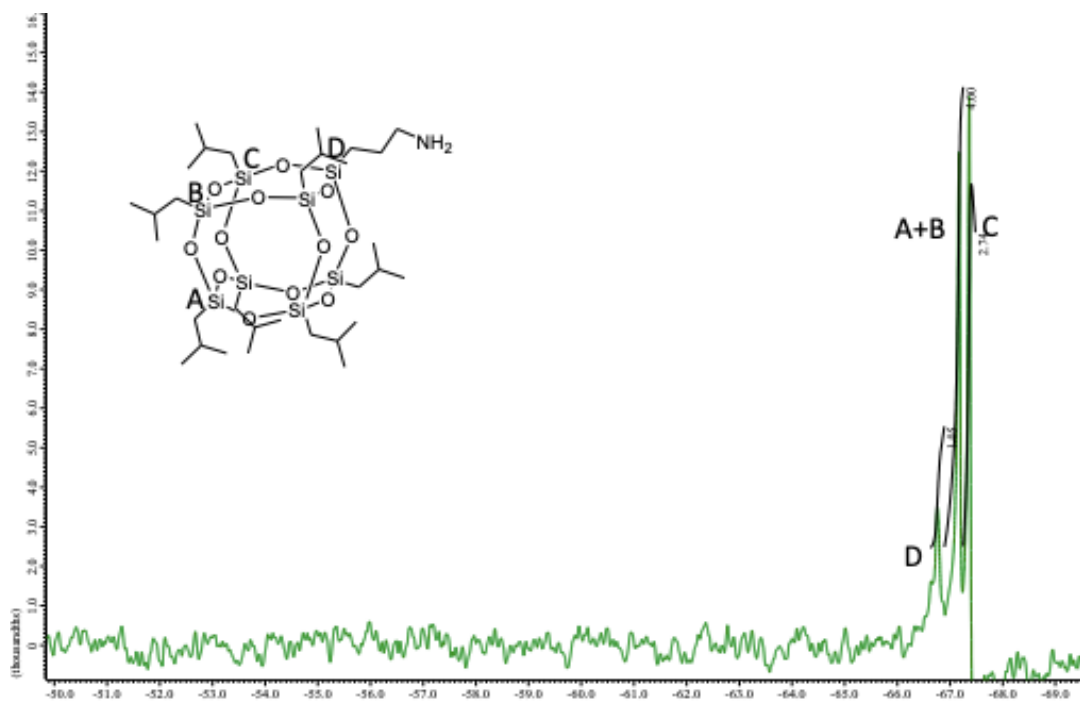


Figure A3. ^{29}Si NMR of AP-IB-POSS. (500 MHz, CDCl_3 , ppm) δ : -66.8, -67.2, -67.4.

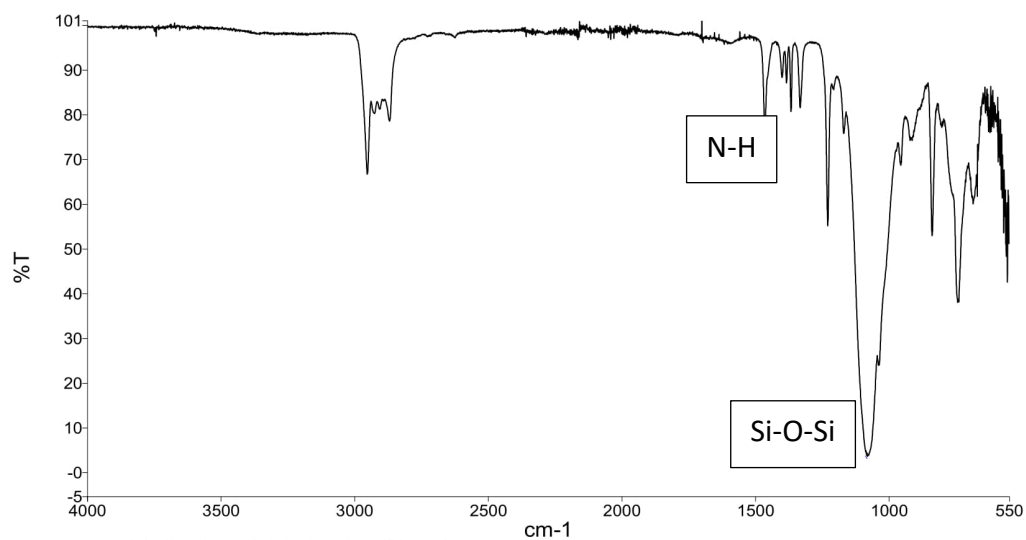


Figure A4. IR of AP-IB-POSS. FTIR (cm^{-1}): 2953, 2906 and 2870 (C-H), 1600 (N-H), 1465 (C-N), 1228 (Si-C), 1081 (Si-O-Si), 955 (Si-O-Si), 740 (Si-C).

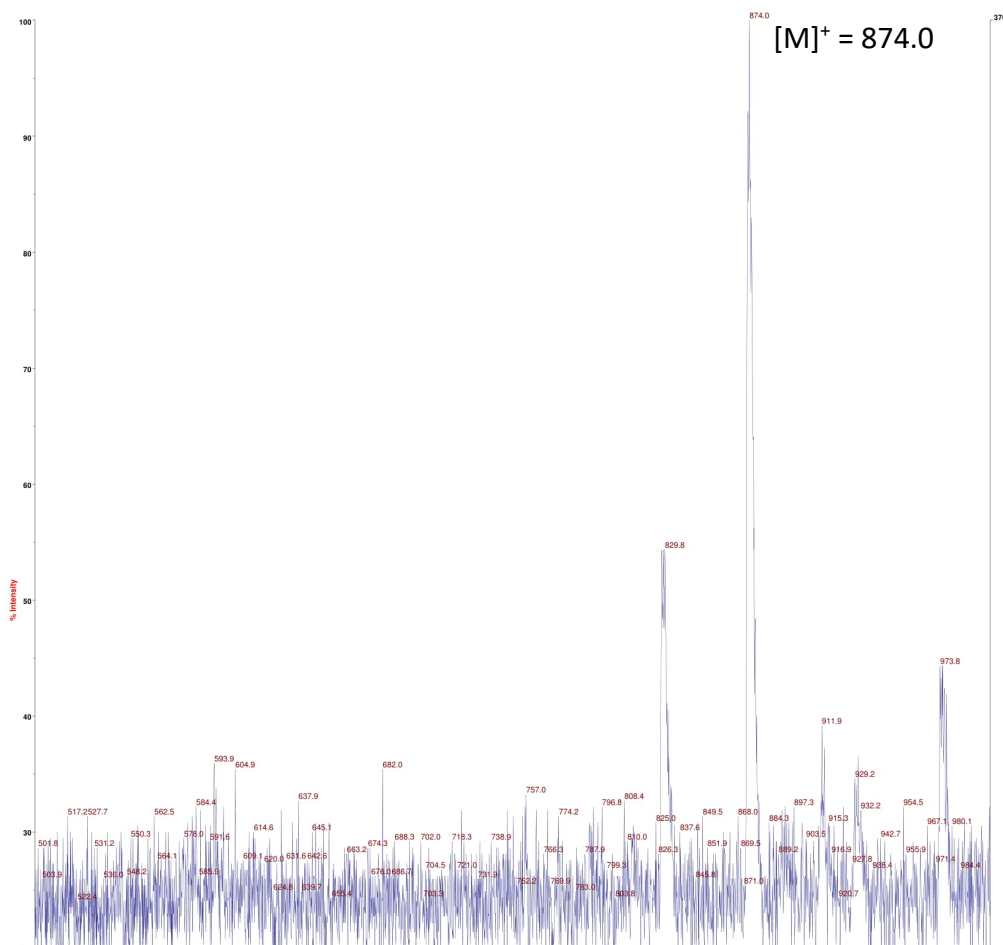


Figure A5. AP-IB-POSS MALDI-TOF (m/z): $[M]^+ = 874.0$ observed; $[M]^+ = 873.31$ calculated.

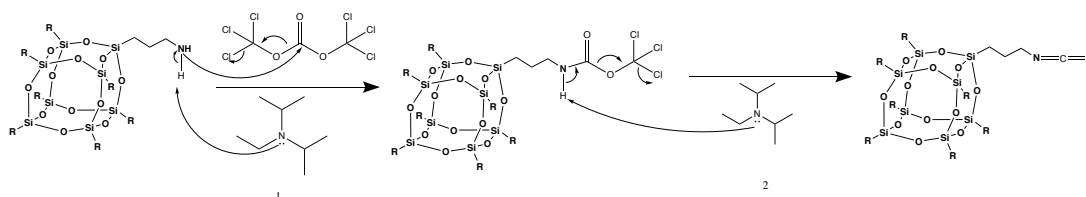


Figure A6. Mechanism of POSS-isocyanate synthesis from hydrophobic-functionalized POSS derivatives under basic conditions.

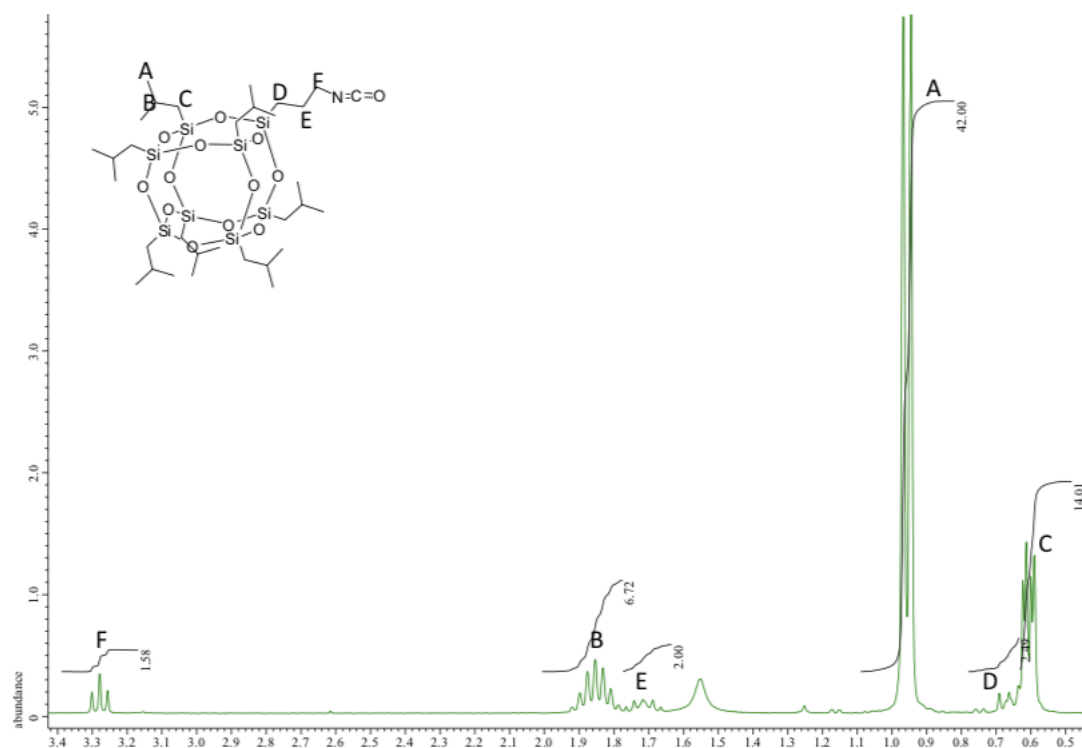


Figure A7. ^1H NMR of IP-IB-POSS. (300 MHz, CDCl_3 , ppm) δ : 3.28 (t, 2H, $-\text{CH}_2-\text{N}=\text{C}=\text{O}$), 1.85 (m, 7H, $-\text{CH}-$), 1.71 (m, 2H, $-\text{CH}_2-$), 0.94 (d, 42H, CH_3), 0.66 (t, 2H, $-\text{Si}-\text{CH}_2-$), 0.60 (m, 14H, $-\text{Si}-\text{CH}_2-$).

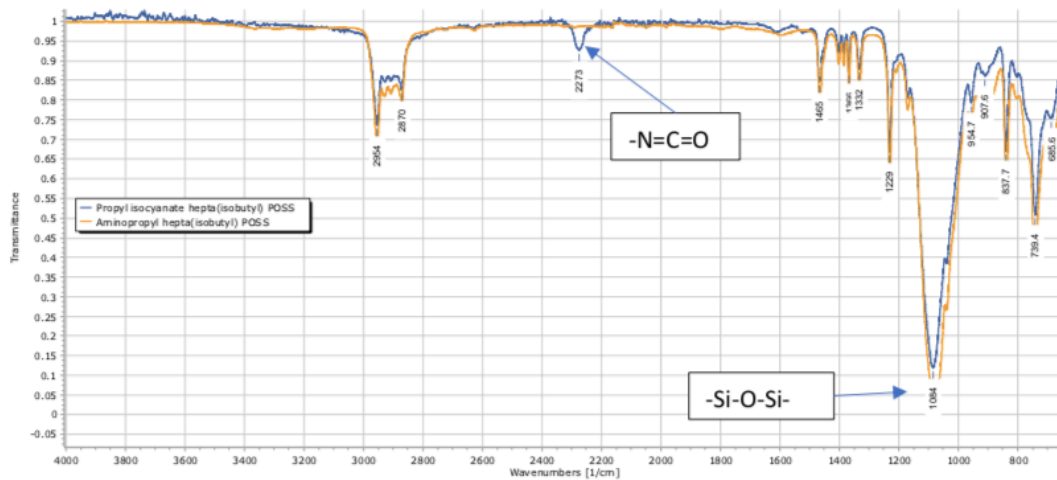


Figure A8. FTIR of IP-IB-POSS compared to AP-IB-POSS. FTIR (cm^{-1}): 2954 and 2870 (C-H), 2273 (N=C=O), 1465 (C-N), 1229 (Si-C), 1084 (Si-O-Si), 955 (Si-O-Si), 739 (Si-C).

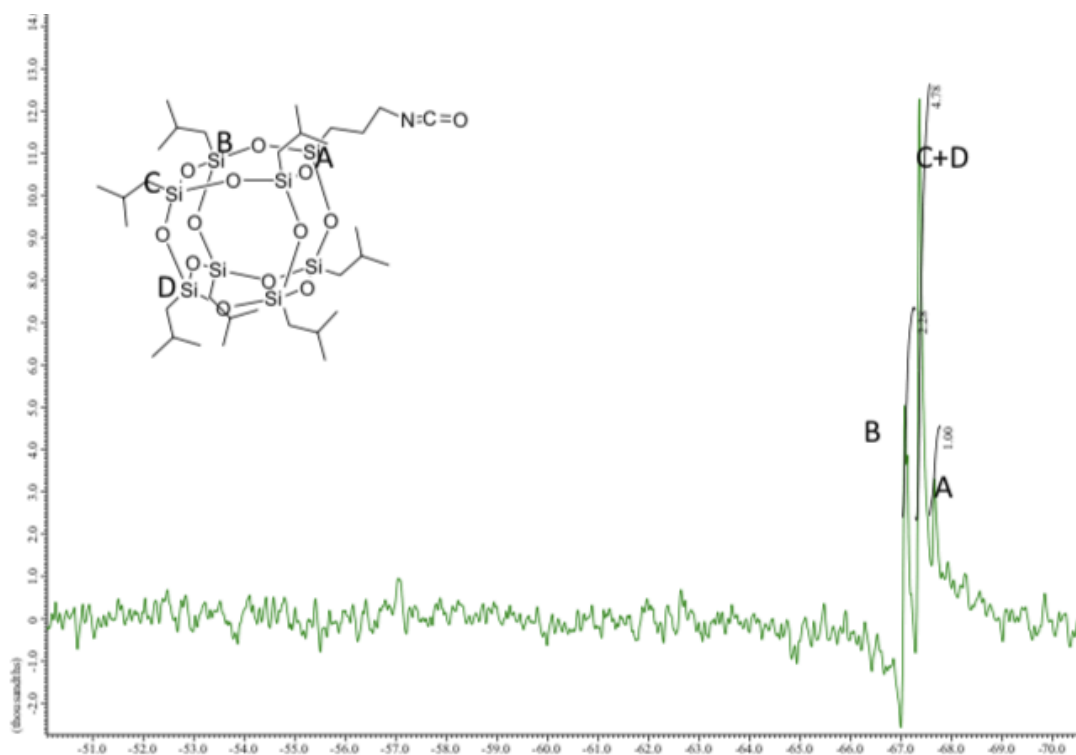


Figure A9. ^{29}Si NMR of IP-IB-POSS. (500 MHz, CDCl_3 ppm) δ : -67.1, -67.4, -67.7.

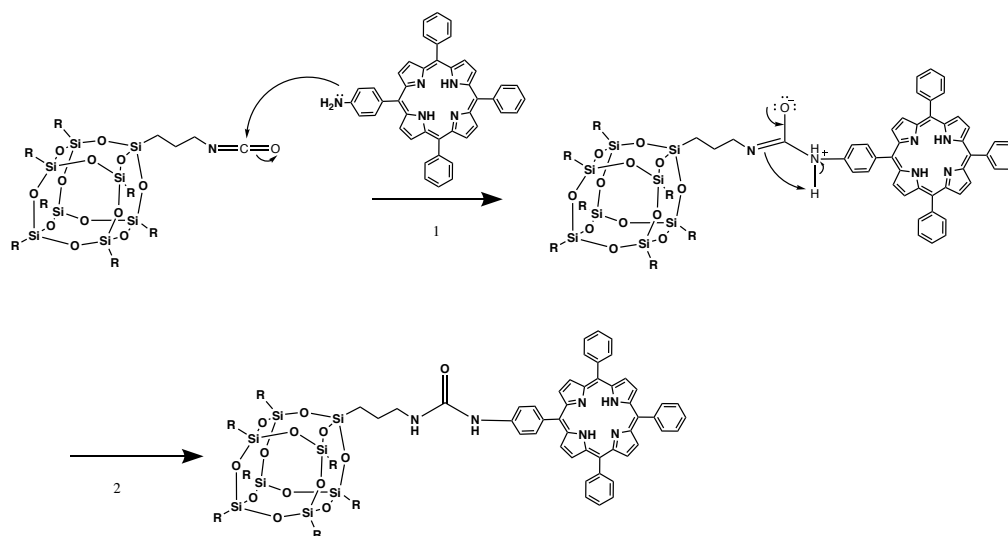


Figure A10. Mechanism of POSS-Porphyrin synthesis from POSS-isocyanate derivatives.

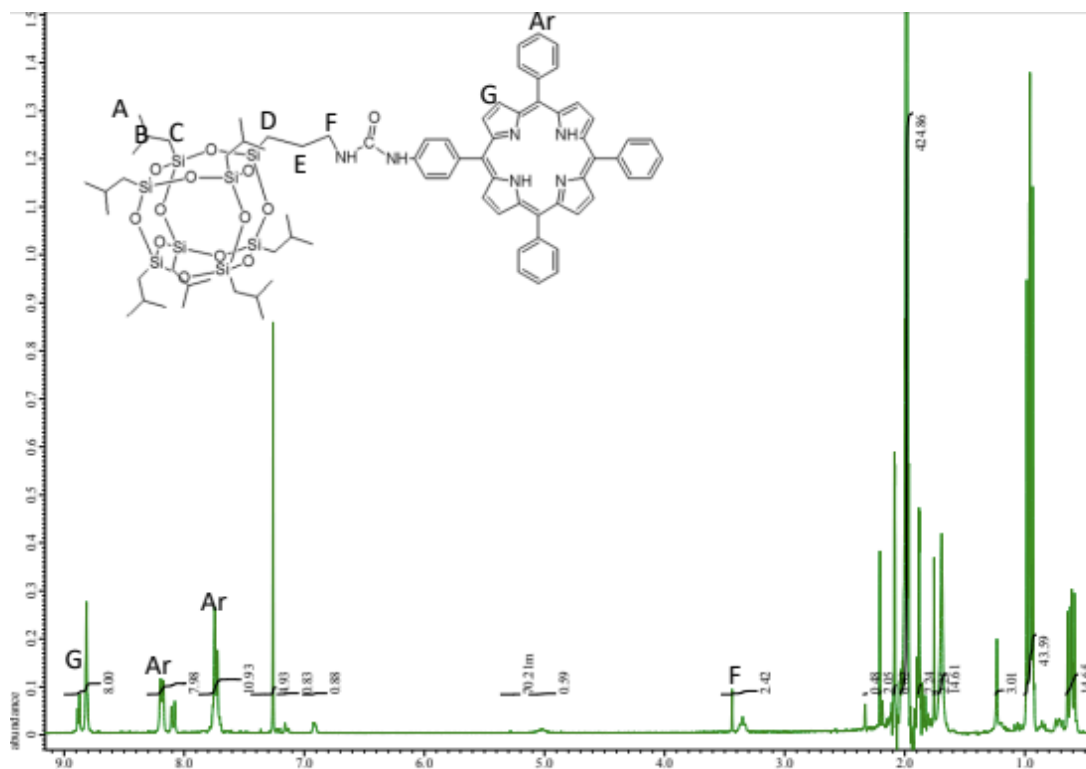


Figure A11. ^1H NMR of IB-POSS-Porphyrin. (300 MHz, CDCl_3 , ppm) δ : 8.87 (m, 8H, Py-H), 8.18 (m, 8H, Ph-H), 7.74 (m, 11H, Ph-H), 3.34 (t, 2H, $-\text{CH}_2\text{-N-}$), 1.88 (m, 7H, $-\text{CH-}$), 1.76 (m, 2H, $-\text{CH}_2\text{-}$), 0.96 (d, 42H, CH_3), 0.71 (t, 2H, $-\text{Si-CH}_2\text{-}$), 0.61 (m, 14H, $-\text{Si-CH}_2\text{-}$).

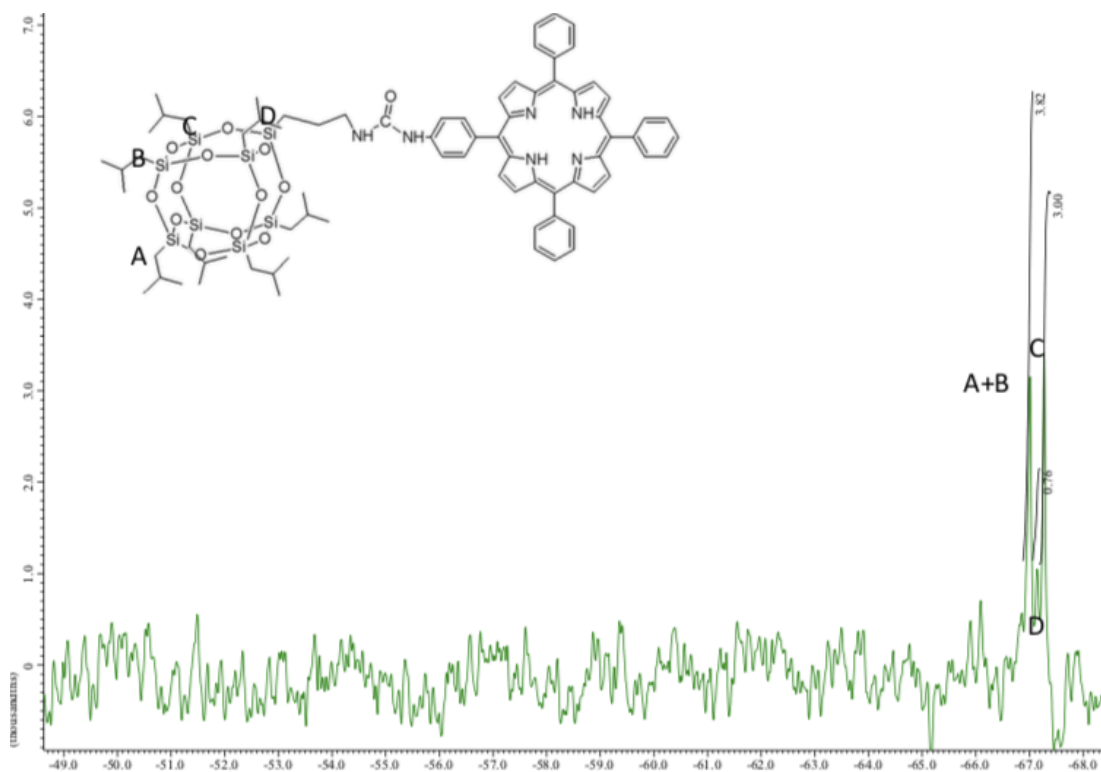


Figure A12. ^{29}Si NMR of IB-POSS-Porphyrin. ^1H -NMR (300 MHz, CDCl_3 , ppm) δ : 8.87 (m, 8H, Py-H), 8.18 (m, 8H, Ph-H), 7.74 (m, 11H, Ph-H), 3.34 (t, 2H, $-\text{CH}_2\text{-N}$ -), 1.88 (m, 7H, $-\text{CH}$ -), 1.76 (m, 2H, $-\text{CH}_2$ -), 0.96 (d, 42H, CH_3), 0.71 (t, 2H, $-\text{Si-CH}_2$ -), 0.61 (m, 14H, $-\text{Si-CH}_2$ -).

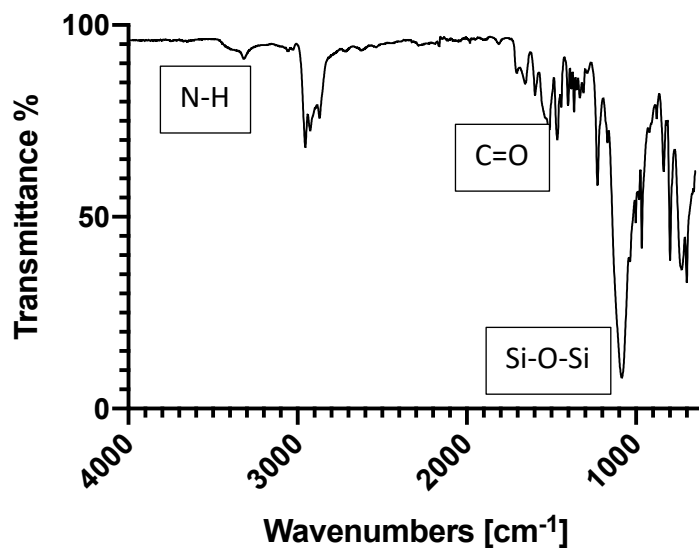


Figure A13. IR of IB-POSS-Porphyrin. FTIR (cm^{-1}): 3318 (N-H), 2925 and 2870 (C-H), 1655 (C=O), 1465 (C-N), 1227 (Si-C), 1084 (Si-O-Si), 966 (Si-O-Si), 700 (Si-C).

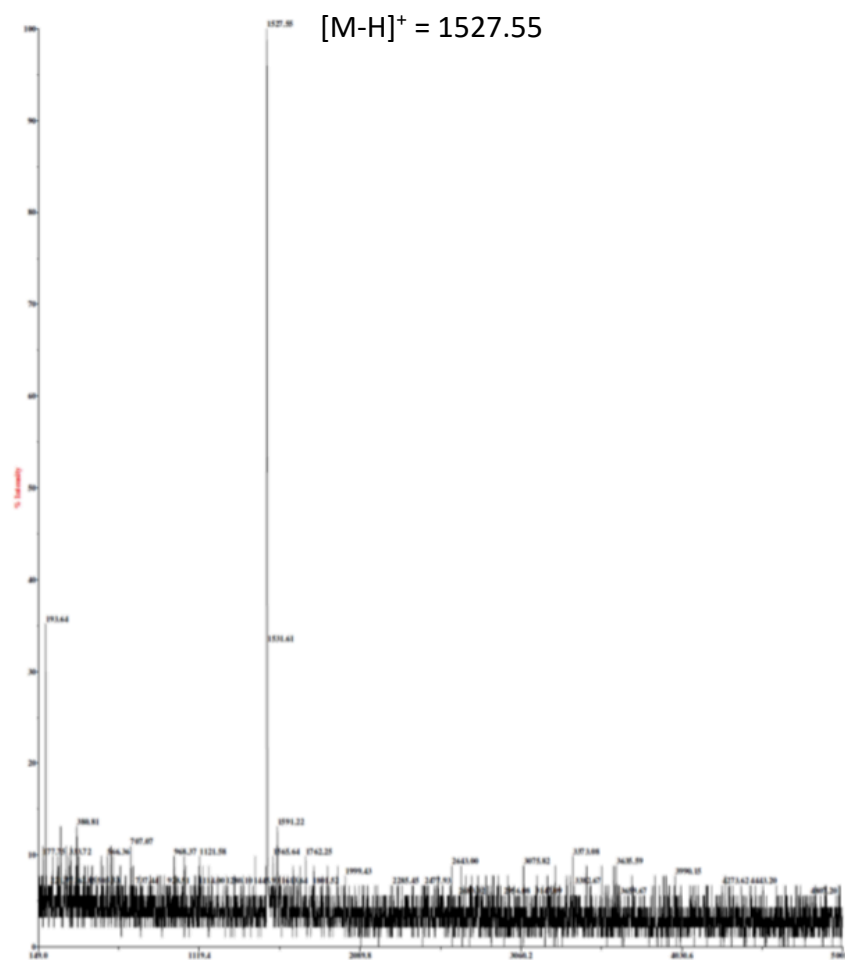


Figure A14. MALDI-TOF of IB-POSS-Porphyrin. (m/z): $[M-H]^+ = 1527.55$ observed; $[M]^+ = 1528.55$ calculated.

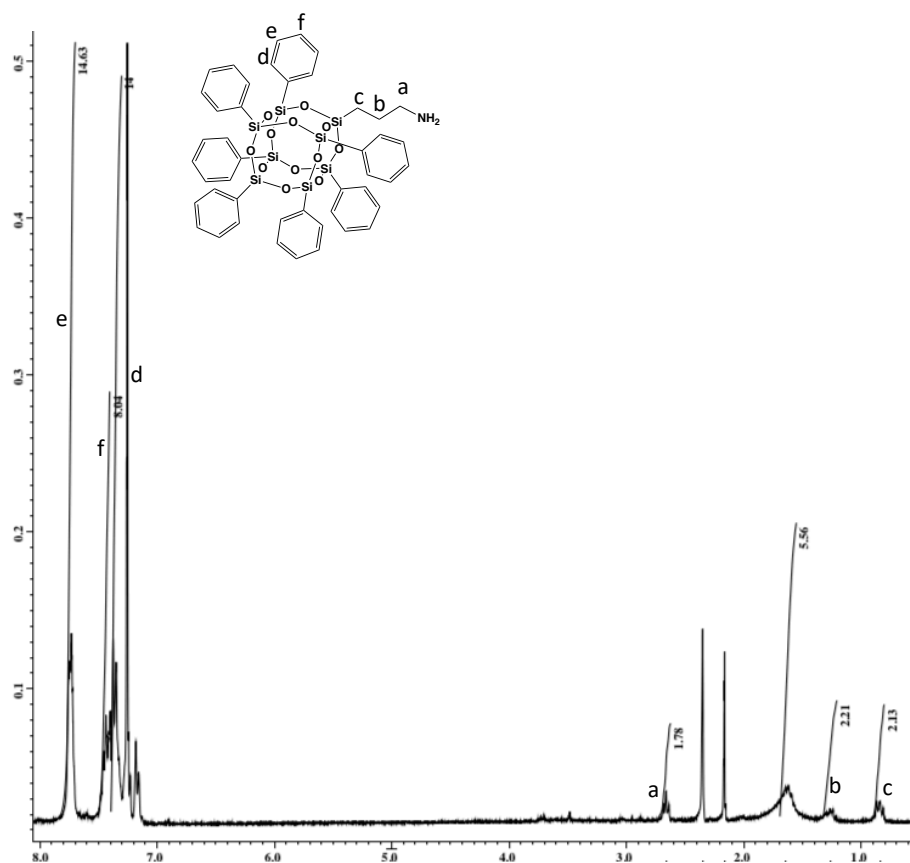


Figure A15. ^1H NMR of AP-Ph-POSS. (300 MHz, CDCl_3 , ppm) δ : 7.74 (m, 14H, Ph-H), 7.44 (m, 7H, Ph-H), 7.37 (m, 14H, Ph-H), 2.66 (t, 2H, $-\text{CH}_2-\text{N}-$), 1.62 (m, 2H, $-\text{CH}_2-$), 0.84 (t, 2H, $-\text{Si}-\text{CH}_2-$). The peaks at 1.5 and 2.2 ppm can be attributed to water and acetone, respectively.

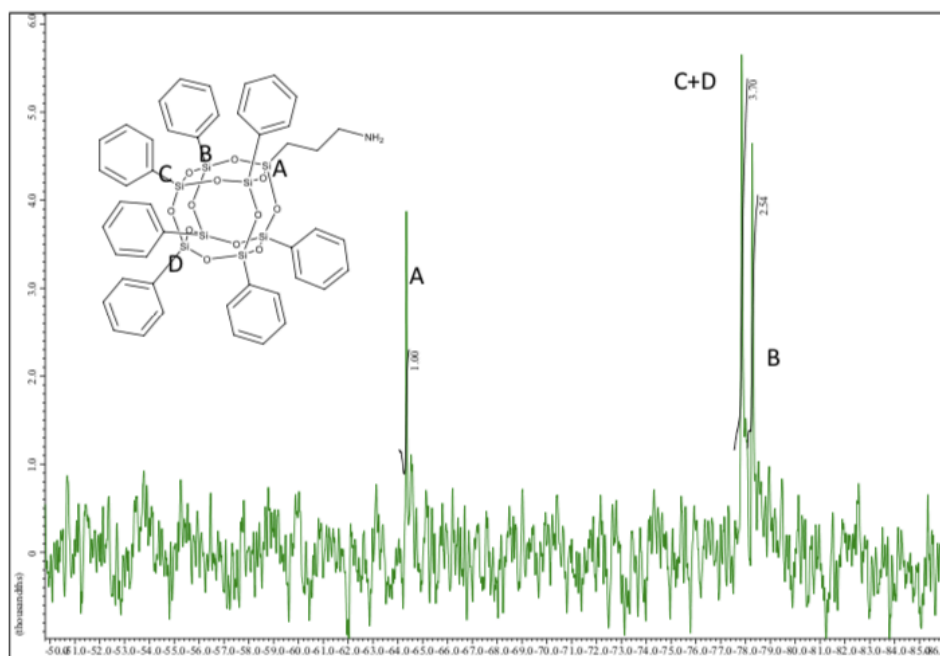


Figure A16. ^{29}Si NMR of AP-Ph-POSS. (500 MHz, CDCl_3 , ppm) δ : -64.5, -77.8, -78.3.

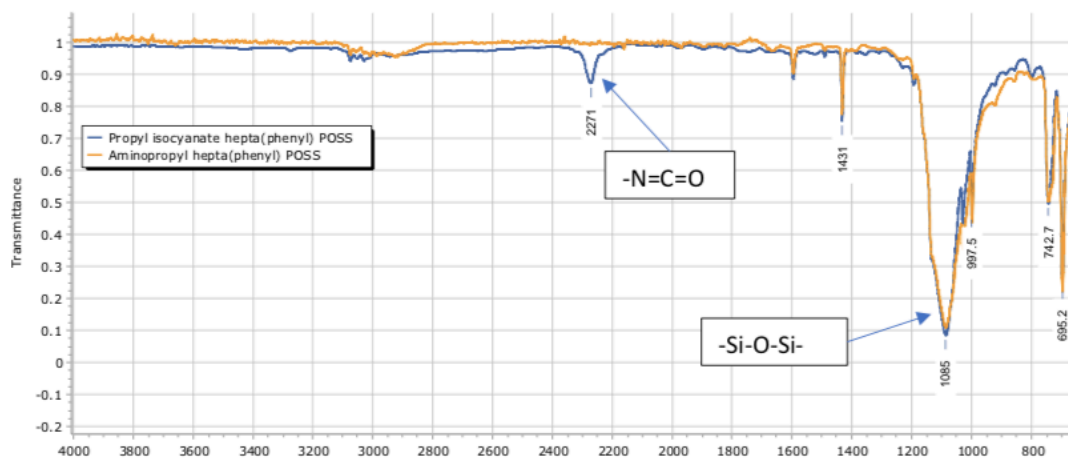


Figure A19. IR of IP-Ph-POSS compared to AP-Ph-POSS. FTIR (cm^{-1}): 3073 (C-H, sp^2), 2933 (C-H, sp^3), 2271 (N=C=O), 1600 (C=O), 1431 (C-N), 1085 (Si-O-Si), 1027 (Si-O-Si), 743 (Si-C).

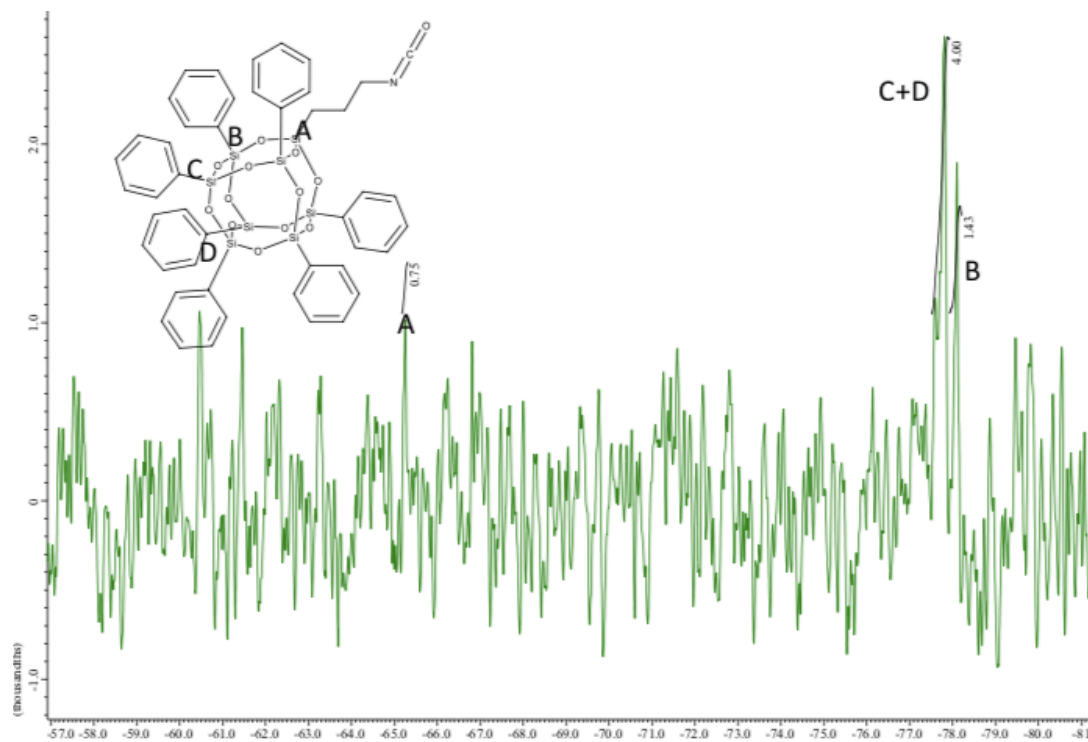


Figure A20. ^{29}Si NMR of IP-Ph-POSS. (500 MHz, CDCl_3 , ppm) δ : -65.3, -77.6, -78.1.

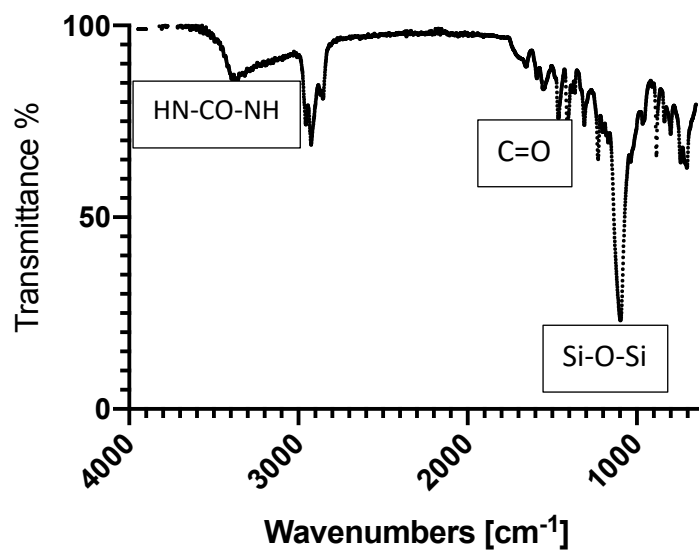


Figure A21. IR of Ph-POSS-Porphyrin. FTIR (cm⁻¹): 3645 (-NH-CO-NH), 3380 (-NH-), 3062 (C-H, sp²), 2960 (C-H, sp³), 1737 (C=O), 1469 (C-N), 1135 (Si-O-Si), 1109 (Si-O-Si), 742 (Si-C).

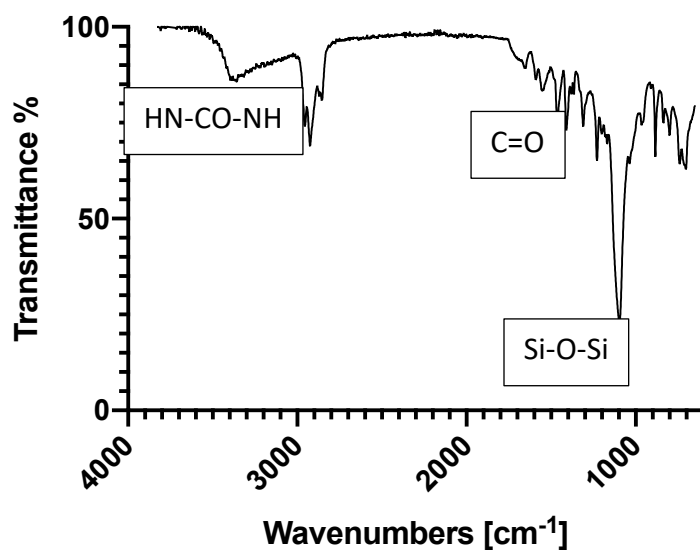


Figure A22. IR of tet(IB-POSS)-Porphyrin. FTIR (cm⁻¹): 3345 (-NH-CO-NH-), 3056 (C-H, sp²), 2922 (C-H, sp³), 1436 (C-N), 1088 (Si-O-Si), 1000 (Si-O-Si), 733 (Si-C).

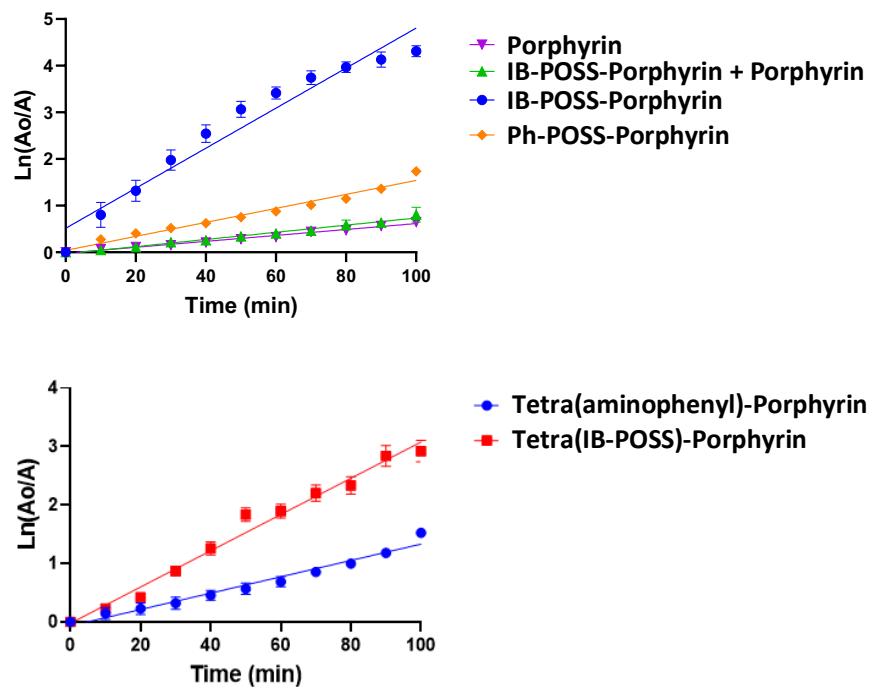


Figure A23. Time-dependent decomposition of DMA plots.

Table A1. Photophysical and photochemical properties of parent porphyrins.

Sample	λ_{Soret} (nm) [$\epsilon \times 10^3$ ($\text{M}^{-1} \text{cm}^{-1}$)] (n=3)	$\lambda_{\text{Emission}}$ (nm)	ϕ_A (n=3)	ϕ_F (n=3)
Porphyrin	419, 275 ± 26 (THF)	661, 745	0.45 ± 0.02	0.21 ± 0.02 (THF)
IB-POSS-Porphyrin	416, 22.1 ± 8.3 (THF)	653, 720	0.82 ± 0.01	0.14 ± 0.01
Ph-POSS-Porphyrin	419, 46.2 ± 9.0 (THF)	653, 719	0.60 ± 0.02	0.13 ± 0.01
Ph-POSS-Porphyrin+ Porphyrin	N/A	N/A	0.53 ± 0.01	N/A
tetra(IB-POSS)-Porphyrin	422, 117.3 ± 34.4 (THF)	663, 719	0.70 ± 0.01	0.13 ± 0.02

Table A2. Partition coefficients.

Compound	Log P_{ow}
Porphyrin	3.18 ± 0.08
Tetra(aminophenyl)porphyrin	1.17 ± 0.06
IB-POSS-Porphyrin	0.62 ± 0.08
Ph-POSS-Porphyrin	0.80 ± 0.04
Tet(IB-POSS)-Porphyrin	-1.10 ± 0.05

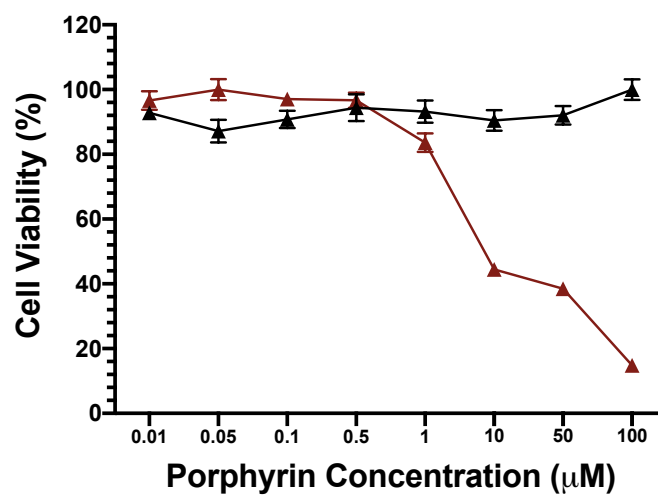


Figure A24. Dose-response curve of Porphyrin treatment to MDA-MB-231 cells for PDT. Red is light treated plate, black is dark (ctrl) plate.

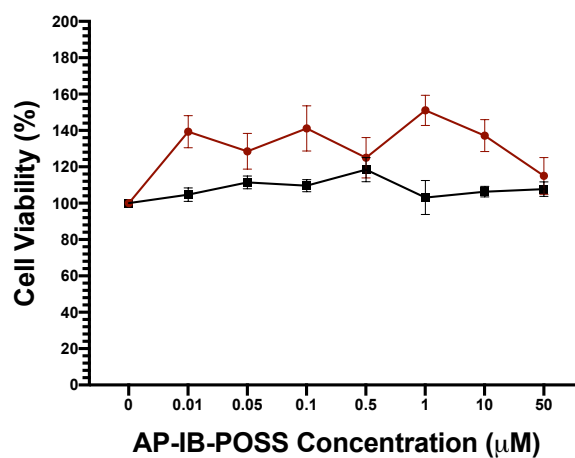


Figure A25. Dose-response curve of AP-IB-POSS treatment to MDA-MB-231 cells for PDT. Red is light treated plate, black is dark (ctrl) plate.

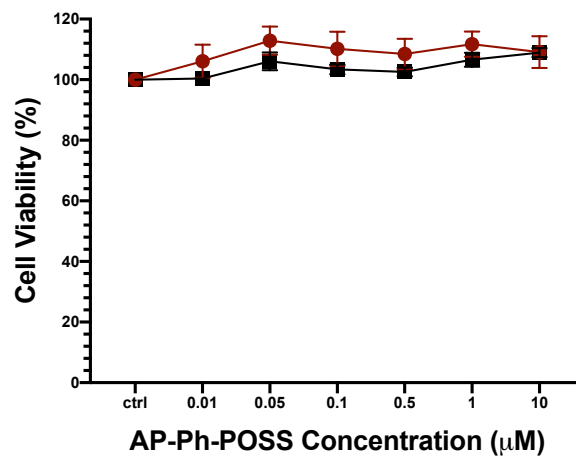


Figure A26. Dose-response curve of AP-Ph-POSS treatment to MDA-MB-231 cells for PDT. Red is light treated plate, black is dark (ctrl) plate.

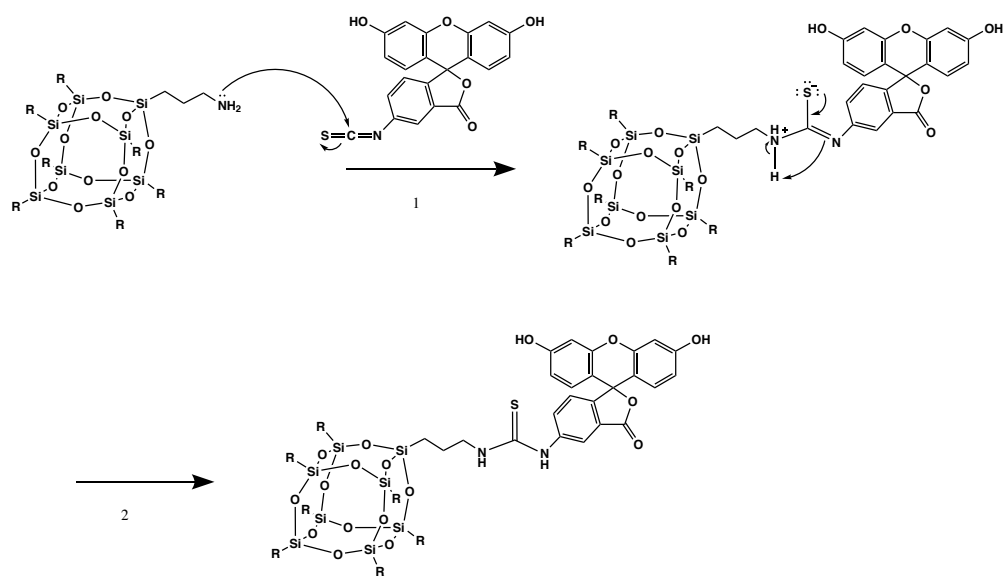


Figure A27. Mechanism of POSS-fluorescein synthesis from POSS derivatives.

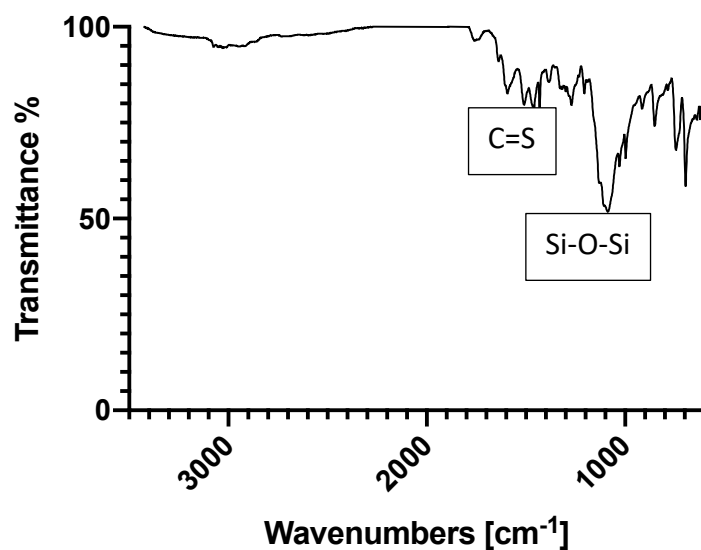


Figure A30. IR of Ph-POSS-fluorescein. FTIR (cm^{-1}): 2589-3627 (COOH stretch), 2925-3074 (sp^3 and sp^2 CH stretch), 1800-1986 (Aromatic overtones), 1255 (C=S stretch), 1089 (Si-O-Si stretch).

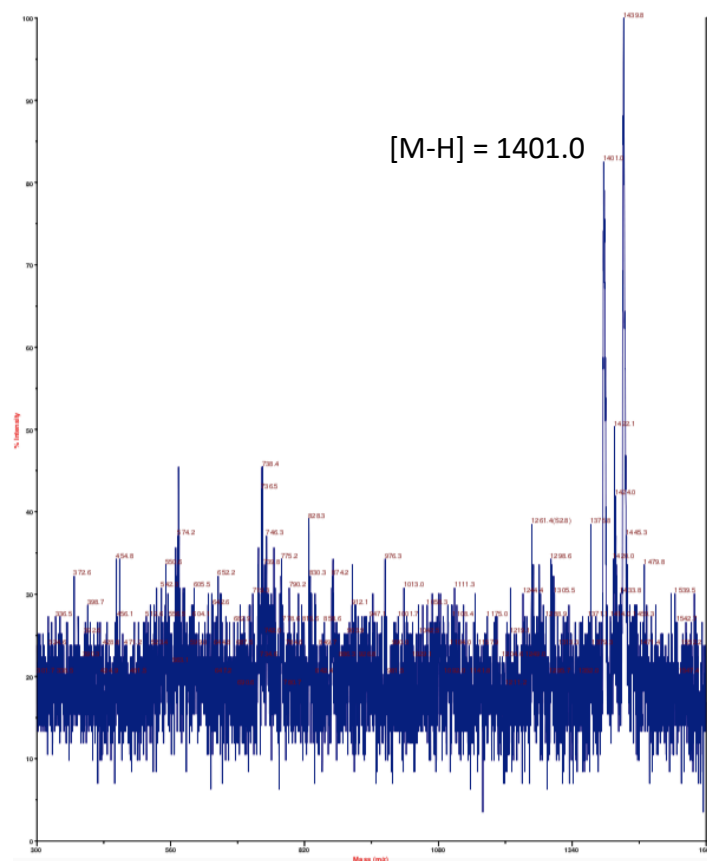


Figure A31. MALDI-TOF of Ph-POSS-fluorescein. (m/z): $[M-H] = 1401.0$, $[M-H+K^+] = 1439.8$ observed, $[M]^+ = 1402.13$ calculated.